



## Statistical state dynamics-based study of the stability of the mean statistical state of wall-bounded turbulence

Brian F. Farrell  and Petros J. Ioannou <sup>\*</sup>

*Department of Earth and Planetary Sciences, Harvard University, Cambridge, Massachusetts 02138, USA*



(Received 12 April 2023; accepted 12 January 2024; published 21 February 2024)

Turbulence in wall-bounded flows is characterized by stable statistics for the mean flow and the fluctuations both for the case of the ensemble and the time mean. Although in a substantial set of turbulent systems, this stable statistical state corresponds to a stable fixed point of an associated statistical state dynamics (SSD) closed at second order, referred to as S3T, this is not the case for wall turbulence. In wall turbulence the trajectory of the statistical state evolves on a transient chaotic attractor in the S3T statistical state phase space and the time-mean statistical state is neither a stable fixed point of this SSD nor, if the time-mean statistical state is maintained as an equilibrium state, is it stable. Nevertheless, sufficiently small perturbations from the ensemble or time-mean state of wall turbulence are expected to relax back to the mean statistical state following an effective linear dynamics. In this work the dynamics of spanwise uniform perturbations to the time-mean flow are studied using a linear inverse model to identify the linear operator governing the ensemble stability of the ensemble or time-mean state by obtaining the time mean stability properties over the transient attractor of the turbulence identified by the S3T SSD. The ensemble or time-mean stability of an unstable equilibrium can be understood by noting that, even when every member of an ensemble is unstable, the ensemble mean may be stable with perturbations following an identifiable stable dynamics. While simplifying insight into turbulent flows has commonly been obtained by identifying and studying ensemble mean statistical states, less attention has been accorded to identifying and studying the ensemble mean dynamics. We show that, in the case of wall turbulence, even though stable fixed-point SSD equilibria are not available to allow application of traditional perturbation analysis methods to identify the perturbation stability of the mean state, an effective linear stability analysis can be obtained to identify the perturbation dynamics of the ensemble or time-mean statistical state.

DOI: [10.1103/PhysRevFluids.9.024605](https://doi.org/10.1103/PhysRevFluids.9.024605)

### I. INTRODUCTION

Turbulence in parallel channel Couette flow (pCf) and pipe Poiseuille flow (pPf) at low Reynolds numbers lies on a transient chaotic attractor in state space [1,2]. However, even in the low Reynolds number simulations used in this work, turbulence persists long enough so that the first two moments of the statistics required by our analysis are converged. The time-mean statistics of the turbulent state in plane Couette flow (pCf) and plane Poiseuille flow (pPf) comprises the time-mean flow  $\langle \mathbf{U} \rangle = U(y)\hat{\mathbf{x}}$ , which is confined to the streamwise direction  $x$  and depends only on the cross-stream direction  $y$  together with the cumulants of fluctuations from this statistical state, which are homogeneous functions of the streamwise and spanwise  $z$  direction. This statistical mean turbulent state depends only on the Reynolds number and is stable in the sense that almost any perturbation

---

<sup>\*</sup>pjioannou@phys.uoa.gr

to the flow will result in the flow relaxing back to its original statistics. If perturbations to the statistical mean state are sufficiently small, the dynamics of these perturbations is expected to be linear and therefore controlled by a linear operator characterized by its eigenmodes and eigenvalues. Recently, the dominant eigenmodes and eigenvalues of the linear operator underlying the dynamics of perturbations to the time-mean velocity profile in turbulent pPf were estimated empirically using a direct numerical simulation (DNS) ensemble by Iyer *et al.* [3] (hereafter referred to as IWCV). IWCV succeeded in estimating the dominant eigenvalues, which characterize the dynamics of relaxation to the time-mean statistical state of all the cumulants of the statistical state, and also the dominant mean-flow eigenmodes, which characterize the least-damped perturbation structures producing relaxation to the time-mean flow.

While statistical stability in the sense of the existence of a stable linear dynamics underlying the return of a perturbed statistical state back to its stationary statistics is expected, and the streamwise and spanwise mean flow component of the first two least stable eigenmodes for the time-mean velocity profile have been estimated, identifying the dynamics of the statistical state stability and its physical mechanism would seem to require solving the statistical state dynamics (SSD) for the full statistical state comprising both the mean state and the higher-order cumulants of the fluctuations, which in the standard ensemble formulation of SSD would require obtaining the dynamics of all the cumulants. Remarkably, this program can be accomplished, to the degree that Gaussian statistics govern the essential dynamics of the SSD, by solving only for the first two cumulants in the appropriate SSD. Using this SSD, referred to as S3T, the statistical stability of the ensemble or time-mean state has been analytically determined in a diverse class of turbulent flows which share the property that the statistical state is attracted to a stable fixed-point equilibrium. The success of this program is predicated on the choice of the averaging operator underlying the S3T SSD. It is important that this averaging operator be the streamwise average, rather than the ensemble average in order that the minimal nontrivial SSD, in which the expansion in cumulants is closed at second order, corresponds to the mechanism of the turbulence. An important attribute of the S3T minimal mechanistically complete SSD is that it provides a Gaussian approximation for all the fluctuation statistics so that, to the extent that Gaussian statistics underlie the fundamental dynamics maintaining wall turbulence, which has been verified [4,5], understanding the mechanism in the transparently simple S3T SSD is tantamount to understanding wall turbulence.

While turbulent systems with stationary statistics are characterized by a statistical equilibrium state to which the trajectory of the ensemble SSD dynamics converges, the corresponding S3T SSD trajectory may identify an underlying transient chaotic attractor, with the dynamics of the approach to the statistical mean state resulting from averaging over this fundamental attractor of the turbulence. Among the turbulent systems for which averaging over the S3T attractor is not required, because the same fixed-point equilibrium is obtained in both the ensemble and the S3T SSD, are two-dimensional (2D)  $\beta$ -plane turbulence [6], three-dimensional (3D) baroclinic turbulence [7,8], drift-wave turbulence in plasmas [9,10], and wall-bounded shear flow in the presence of free-stream fluctuations but before transition to self-sustaining turbulence (referred to as pretransitional flow) [11,12]. In these cases the stability of the S3T time-mean state, which coincides with the ensemble mean state, can be determined by eigenanalysis of the S3T operator perturbed about the time-mean state. In wall-bounded flows after transition to turbulence (referred to as post-transitional flow) no stable fixed points of the S3T SSD exist and the S3T state trajectory lies on the fundamental transient chaotic attractor of wall turbulence that it identifies [11,12]. Therefore, the program of analytically determining the stability of the statistical state of a post-transitional turbulent shear flow by finding and perturbing the fixed point of its S3T SSD equations fails. It is useful to comment on some implications of this result:

(1) The instability of the ensemble or time mean state identified in the S3T SSD is a physical instability that can be observed in Navier-Stokes (NSE) turbulence. It is a member of a set of nonlinear instabilities resulting from interaction between the mean shear flow and fluctuations to the mean shear flow. S3T allows analytic expression to be obtained for this class of instabilities in turbulent shear flow [6,11–22].

(2) There is no contradiction arising from the required stability of the ensemble or time mean state in ensemble dynamics and its instability when considered in S3T dynamics. Stability of the ensemble mean state is implied by stationarity of the statistics of the turbulent flow and can occur even when each member of the ensemble is unstable as consideration of the stochastically modulated Mathieu equation governing the ensemble evolution of the parametric mass-spring example shows. In that example every ensemble member is unstable while the ensemble mean has stable limit cycle dynamics [23].

(3) The lack of a stable fixed point in S3T dynamics corresponding to the ensemble or time-mean flow implies the nonexistence of a point attractor. In these cases the pertinent dynamics needs to be obtained by ensembling over the transient chaotic attractor. The emergent dynamics obtained by averaging over this attractor can be an object of study analogous to studying the ensemble mean statistics of the turbulent state. For example, consider that a covariance matrix and a lag covariance matrix have been obtained from observations of a turbulent flow. Each of these is a statistical quantity and the object of traditional study by ensemble methods. However, the mapping between them is a linear operator related directly to the dynamics of the turbulence rather than to its statistical state. It is this emergent ensemble dynamical object that provides insight into turbulence.

(4) The dynamics of the S3T SSD is chosen explicitly to isolate the essential components of turbulence dynamics: the mean flow, the second cumulant, and the interaction between them. In contrast to the familiar concept of the turbulent state as a point moving along a chaotic trajectory lying on an attractor embedded in the state space of velocity [24], the SSD viewpoint, is of turbulence as a point moving along a chaotic trajectory in the SSD state space with coordinates the mean flow and the higher velocity cumulants. Remarkably, the essential dynamics of wall turbulence is obtained using the simplest nontrivial closure, the S3T SSD, which retains only the first and second cumulants. It is useful for visualization purposes to translate the state space of this second-order closure to velocity variables in which the mean flow point (first cumulant) and its surrounding probability distribution of fluctuations (second cumulant) follows a chaotic trajectory. The probability distribution obtained from the covariance matrix of the second cumulant in S3T SSD is multivariate Gaussian while the exact distribution, which can be obtained by closing with the third cumulant from a DNS, is slightly non-Gaussian. The iso-density locus of the multivariate Gaussian probability density function (PDF) forms an elliptical distribution. The axes and orientation of this elliptical distribution determine the Reynolds stresses that, together with the nonlinear mean flow dynamics, determine the chaotic trajectory in the state space of the SSD. Adopting this SSD state space chaotic attractor viewpoint of turbulence dynamics is motivated further by the observation that wall turbulence at high Reynolds numbers can be regarded as a covering (tiling) of the turbulent channel with minimal channel units [25–27], the dynamics of each of which is closely approximated by a minimal channel S3T SSD, to form an ensemble covering of the attractor that would have ensemble mean dynamics equivalent to the time mean dynamics obtained by time integration over one of these units. A related study recently showed that displacing the observed minimal channel tiles in a DNS of wall turbulence, so that the roll-streak structure in the tiles is aligned in the streamwise direction, recovered the S3T dynamics. Given that the roll-streak structures so aligned have wave number zero in the streamwise direction, as required in the S3T formalism, verifies that the S3T SSD dynamics, which is associated with an analytically characterized transient chaotic attractor in SSD state space, is also relevant to understanding wall turbulence at high Reynolds number [28,29].

(5) While there are differences in the statistical distributions obtained between DNS and S3T [30–32], these differences arise in conjunction with the simplification of the dynamics of S3T SSD that allows detailed analysis of the mechanism underlying the turbulence and the fact that these differences do not affect the fundamental dynamics (e.g., SSP cycle, wall stresses, mean velocities [4,5,33]) indicates that these differences are inessential.

It should be additionally noted that the attractor of the S3T SSD in cumulant variables differs from the attractor of the corresponding turbulent state represented in its velocity variables. For example, in beta-plane turbulence the turbulent state in velocity variables follows a chaotic trajec-

tory, while in the corresponding S3T SSD expressed in its statistical state cumulant variables the attractor is most often a stable fixed point, the stability properties of which can be obtained using standard stability analysis [13]. Post-transitional wall turbulence presents a case in which both the S3T SSD in cumulant variables and the turbulent state in velocity variables lie on distinct transient chaotic attractors. In this case the ensemble stability properties of the S3T SSD can be obtained by invoking ergodicity and averaging over the S3T SSD chaotic trajectory. An alternative is to exploit ergodicity by seeding an ensemble of perturbations over the reflection of the S3T attractor in DNS in order to explore its ensemble stability properties, as in the analysis of IWCV. Agreement between these very different conceptual and computational approaches lends credence to the view of an emergent ensemble stability dynamics arising as an average dynamics, the average being taken over an attractor whether it be through ensemble or time averaging. It also lends support to viewing turbulence as lying on an attractor in statistical state space distinct from the traditional attractor in velocity space [24].

To properly interpret stability analysis applied to statistical states, it is important to distinguish the instability of an SSD state in cumulant variables from the more familiar hydrodynamic instability of a flow state in velocity variables. In linear hydrodynamic stability studies, an unperturbed flow state is maintained while growth or decay of perturbations to this flow is examined. For example, in the absence of fluctuations, laminar pCf is an equilibrium state and the associated linear perturbation equation has eigenvalues with negative real part indicating the pCf is hydrodynamically stable to infinitesimal perturbations at all Reynolds numbers. By contrast, SSD stability examines the stability of the cumulants, which are the state variables of the SSD equations (cf. Refs. [13,34,35]). Linear SSD stability analysis subsumes linear hydrodynamic stability analysis: in the absence of background fluctuations producing nonvanishing higher-order cumulants, the hydrodynamic stability of the associated laminar flow assures also its SSD stability. However, the SSD equations may also support additional instabilities when the flow state contains a nonvanishing second-order cumulant. These instabilities arise from the interaction between perturbations to the mean flow and the second cumulant of the unperturbed SSD state, which is absent in hydrodynamic stability analysis. This interaction is familiar because it underlies the self-sustaining process in wall-bounded flows [36,37]. It is important to note that the S3T SSD, which incorporates quadratic variables, allows us to determine using linear eigenanalysis the existence of this set of nonlinear instabilities supported by the NSE in wall-bounded shear flow. An example of such a nonlinear instability arises in stationary spanwise independent mean flow equilibria maintained by a spanwise homogeneous field of turbulent fluctuations in the S3T SSD of pCf. These spanwise independent mean flow equilibria are SSD unstable for sufficiently high Reynolds number and in the presence of sufficient stochastically maintained turbulence both in the framework of the S3T SSD [11], and by DNS ensemble approximations to an SSD closed at infinite order [12]. The unstable modes that arise from the SSD instability of these spanwise independent SSD mean flow equilibria have the form of streamwise roll-streak structures that break the spanwise homogeneity of the streamwise and spanwise independent SSD equilibrium state. Importantly, over a range of Reynolds numbers and levels of stochastically maintained turbulence, these instabilities equilibrate to form stable finite amplitude fixed point states with roll-streak (R-S) structure. The stability of these R-S states was verified by study of the perturbation dynamics of these SSD equilibria [12]. However, for high enough Reynolds numbers and levels of stochastically excited turbulence, there is no stable fixed point equilibrium statistical state and the statistical state of the turbulence lies on a transient chaotic attractor. Turbulence, once established on this attractor of the statistical state, continues to be maintained when the stochastic excitation responsible for its inception is removed, indicating that the turbulence is self-maintained absent typically rare relaminarization events [5,11]. In this work we show, within the framework of the S3T SSD, that the time-mean flow that is self-maintained in turbulent pCf is S3T unstable with eigenmodes in the form of streamwise R-S structures together with supporting perturbations in the form of the second-order cumulant.

At this point in our study we will have verified that the statistical mean state of turbulent pCf is neither a state of marginal hydrodynamic stability nor is it a state of S3T SSD stability, rather it is SSD unstable to structures with the R-S form, which leaves open the question of explaining and quantifying the observed statistical stability of the time-mean flow in pCf. That a physical instability of the time-mean state is verified in this paper to exist in the S3T SSD suffices to ensure that this mean flow is not a fixed point about which traditional time-independent stability analysis to obtain eigenmodes and eigenvectors can be applied. Nevertheless, perturbation stability of any SSD with stationary statistics is expected. The first step in the analysis of the origin and nature of the expected linear stability of a time-mean flow would be to obtain the eigenvalues and eigenmodes of the necessarily linear dynamics of streamwise and spanwise constant perturbations to this time-mean flow. In pPf turbulence, IWCV used an ensemble method to obtain empirically the first two eigenvalues and eigenmodes of this linear dynamics. An open question is what this stable empirical linear dynamics represents. To address this question we have obtained an effective linear dynamics governing perturbations to the time-mean statistical state in a quasilinear pCf, and in a pPf DNS, which makes connection with IWCV. The effective linear dynamics was obtained using linear inverse modeling (LIM), which has been applied widely in geophysical fluid dynamics [38–41]. An early application of LIM was to diagnose the mechanism and predict the evolution of the El-Niño Souther Oscillation in the Tropical Pacific [40,42]. In addition, the LIM was used to determine the effective dynamics governing the climate statistics of an atmospheric model [43] and the low-frequency variability of the midlatitude climate [44]. In another application, LIM analysis was used to show that the eddy stresses interacting with the mean flow in two-layer quasigeostrophic turbulence can be diagnosed to comprise the action of upgradient momentum transport together with eddy-diffusion and stochastic excitation [45]. In an early application to fluid dynamics, the LIM was used to show that the dynamics of a dilute gas in a Rayleigh-Bénard configuration near criticality reproduces the linearized NSE excited with stochastic forcing with the covariance predicted by the Landau-Lifschitz theory [46].

LIM analysis infers the dynamics of fluctuations about the time-mean state from the covariance and the time advanced covariance of the fluctuations exploiting ergodicity to interpret the linear dynamics obtained as the ensemble linear dynamics over the transient chaotic attractor. In both the LIM time-mean method and the IWCV ensemble-mean method, the eigenvalues and eigenmodes of perturbations from the time-mean flow correspond to the temporal evolution and structure of the least damped modes governing return to the stable stationary fixed point of the ensemble SSD.

It is instructive to note that, LIM analysis addresses the issue of providing the optimal linear operator and excitation for resolvent analysis. In resolvent analysis the operator of the linear dynamics is prescribed to be the operator that governs the evolution of perturbations about the time-mean, possibly modified by eddy viscosity [30,47,48], and the accuracy of the predictions of resolvent analysis is predicated on the structure and spectrum of the input excitations, which is a topic being actively researched (cf. Zare *et al.* [49], Towne *et al.* [50], Bae *et al.* [51], Morra *et al.* [52], Holford *et al.* [53], Holford and Hwang [54], and Abootorabi and Zare [55]). LIM obtains the Langevin form of the ensemble perturbation dynamics that resolvent analysis relies upon including both the operator of the linear dynamics and the covariance of the associated excitation. From this perspective LIM can be viewed as providing a method for constructing the optimal linear model for the dynamics of fluctuations in turbulence in which the ambiguity in the structure of the excitation has been resolved.

We conclude that, in post-transitional wall turbulence, no stable fixed point exists that would correspond to the stable fixed points of the S3T SSD in the pretransitional turbulent state, which allowed the modes to be identified directly by perturbing the SSD dynamics linearized about this stable stationary point. However, nothing essential is lost, insofar as the dynamics of perturbations to the time-mean flow is concerned, as the LIM and ensemble methods both allow the effective linear dynamics of perturbations to the time-mean flow averaged over the fundamental structure of the transient chaotic attractor to be identified.

## II. FORMULATION OF THE S3T STATISTICAL STATE DYNAMICS STABILITY ANALYSIS FOR WALL TURBULENCE

Consider a pCf with streamwise direction  $x$ , wall-normal direction  $y$ , and spanwise direction  $z$ . The lengths of the channel in the streamwise, wall-normal, and spanwise direction are respectively  $L_x$ ,  $2h$ , and  $L_z$ . The channel walls are at  $y/h = -1$  and  $1$ . Averages are denoted by angle brackets with a subscript denoting the independent variable over which the average is taken, i.e., streamwise averages by  $\langle \cdot \rangle_x = L_x^{-1} \int_0^{L_x} \cdot dx$ , time averages by  $\langle \cdot \rangle_t = T^{-1} \int_0^T \cdot dt$ , and ensemble averages over different realizations of the flow obtained from different initial conditions by  $\langle \cdot \rangle_E$ . To proceed with the formulation of the S3T SSD closed at second order we choose as an averaging operator the streamwise mean. This is a crucial choice because it allows the formulation of a second-order mean-field theory that supports realistic turbulence, including in pCf and pPf [5,11]. In this closure the vector velocity  $\mathbf{u}$  is decomposed into its streamwise mean, denoted  $\mathbf{U}(y, z, t)$ , and the deviation from this mean (the fluctuations), denoted  $\mathbf{u}'(x, y, z, t)$ , so that  $\mathbf{u} = \mathbf{U} + \mathbf{u}'$ . The pressure gradient is similarly decomposed as  $\nabla p = \nabla [P(y, z, t) + p'(x, y, z, t)]$ . Velocity is nondimensionalized by the velocity at the wall,  $U_w$ , at  $y/h = 1$ , lengths by  $h$ , and time by  $h/U_w$ . The nondimensional NSE decomposed into an equation for the mean and an equation for the fluctuations are

$$\partial_t \mathbf{U} + \mathbf{U} \cdot \nabla \mathbf{U} + \nabla P - \Delta \mathbf{U} / \text{Re} = -\langle \mathbf{u}' \cdot \nabla \mathbf{u}' \rangle_x, \quad (1a)$$

$$\partial_t \mathbf{u}' + \mathbf{U} \cdot \nabla \mathbf{u}' + \mathbf{u}' \cdot \nabla \mathbf{U} + \nabla p' - \Delta \mathbf{u}' / \text{Re} = -\langle \mathbf{u}' \cdot \nabla \mathbf{u}' - \langle \mathbf{u}' \cdot \nabla \mathbf{u}' \rangle_x \rangle, \quad (1b)$$

$$\nabla \cdot \mathbf{U} = 0, \quad \nabla \cdot \mathbf{u}' = 0. \quad (1c)$$

where  $\text{Re} = U_w h / \nu$  is the Reynolds number. The velocities satisfy periodic boundary conditions in the  $z$  and  $x$  directions and no-slip boundary conditions in the cross-stream direction:  $\mathbf{U}(x, \pm 1, z, t) = (\pm 1, 0, 0)$ ,  $\mathbf{u}'(x, \pm 1, z, t) = 0$ .

The S3T SSD, which is based on the crucial choice of a streamwise mean for the averaging operator, when closed at second order embodies the fundamental dynamics underlying wall turbulence. It is the S3T SSD that allows analytic solutions to be found and makes direct connection to canonical cumulant expansion methods and insights. A highly accurate second-order cumulant approximation to the S3T SSD that provides motivation for deriving the S3T SSD as well as a powerful computational tool can be directly obtained from the quasilinear approximation of Equation (1):

$$\partial_t \mathbf{U} + \mathbf{U} \cdot \nabla \mathbf{U} + \nabla P - \Delta \mathbf{U} / \text{Re} = -\langle \mathbf{u}' \cdot \nabla \mathbf{u}' \rangle_x, \quad (2a)$$

$$\partial_t \mathbf{u}' + \mathbf{U} \cdot \nabla \mathbf{u}' + \mathbf{u}' \cdot \nabla \mathbf{U} + \nabla p' - \Delta \mathbf{u}' / \text{Re} = 0, \quad (2b)$$

$$\nabla \cdot \mathbf{U} = 0, \quad \nabla \cdot \mathbf{u}' = 0, \quad (2c)$$

which entails neglecting or parametrizing the fluctuation-fluctuation interactions in (1b) while retaining the fluctuation-fluctuation interactions in (1a) (cf. Refs. [11,35,56,57]). Here we neglect altogether the fluctuation-fluctuation interactions in (1b). Neglecting altogether the fluctuation-fluctuation interactions in (1b) has no fundamental effect on the turbulence in the sense that the turbulent state is supported with the mean and integral scales as well as the energy-extracting scales of the fluctuations being similar to those of a DNS of pCf. This quasilinear system, which approximates the S3T SSD, is referred to as the restricted nonlinear system (RNL) (cf. Refs. [4,58–60]). It is worth noting that the underlying dynamical structure of the quasilinear equations has been verified by Alizard [61], Alizard and Biau [62], and Pausch *et al.* [63] to support edge states and to have the bifurcation behavior of exact coherent structures of the Navier-Stokes equations.

The S3T SSD describes the composite dynamics resulting from the interaction of an ensemble of fluctuations, each of which evolves under the same streamwise-mean flow  $\mathbf{U}$ , with the streamwise-mean flow. This choice of adopting the streamwise average in the S3T SSD formulation is physically motivated: this SSD captures the essential dynamics of the turbulence at second order, which are the self-sustaining process and its regulation. The variables of the S3T SSD are the first two cumulants

consisting of the streamwise mean flow,  $\mathbf{U} = (U, V, W)$  or  $\mathbf{U} \stackrel{\text{def}}{=} (U_x, U_y, U_z)$ , and the second-order cumulants that are the same time ensemble mean covariances of the Fourier components of the velocity fluctuations,  $\hat{u}'_{\alpha, k_x}$ , where the index  $\alpha = x, y, z$  indicates the velocity component in the Fourier expansion of the perturbation velocity  $\mathbf{u}'$ :

$$\mathbf{u}'(x, y, z, t) = \sum_{k_x > 0} \Re(\hat{\mathbf{u}}'_{k_x}(y, z, t)e^{ik_x x}). \quad (3)$$

The second-order cumulant variables are the ensemble mean covariances of the velocity components of Fourier component  $k_x$  between point 1  $\stackrel{\text{def}}{=} (y_1, z_1)$  and point 2  $\stackrel{\text{def}}{=} (y_2, z_2)$  evaluated at the same time:

$$C_{\alpha\beta, k_x}(1, 2) = \langle \hat{u}'_{\alpha, k_x}(1) \hat{u}'_{\beta, k_x}{}^*(2) \rangle_E, \quad (4)$$

which is a function of the coordinates of the two points (1) and (2) on the  $(y, z)$  plane and of time ( $*$  denotes complex conjugation). The SSD equations corresponding to the second-order closure of (2) are obtained by identifying the Reynolds stress forcing term  $\langle \mathbf{u}' \cdot \nabla \mathbf{u}' \rangle_x$  in (1a) with its ensemble mean,  $\langle \langle \mathbf{u}' \cdot \nabla \mathbf{u}' \rangle_E \rangle_x$ , with the fluctuations taken from the same mean  $\mathbf{U}$ . The equation for the second-order cumulant can be obtained by time differentiating the covariance (4) and using (2b) (for a derivation, see Refs. [6,14,35]). The SSD equations in this second-order closure are

$$\partial_t U_\alpha + U_\beta \partial_\beta U_\alpha + \partial_\alpha P - \Delta U_\alpha / \text{Re} = -\frac{1}{2} \sum_{k_x} \Re(\partial_{\beta, 1} C_{\alpha\beta, k_x}(1, 2))_{1=2}, \quad (5a)$$

$$\partial_t C_{\alpha\beta, k_x}(1, 2) = A_{\alpha\gamma, k_x}(1) C_{\gamma\beta, k_x}(1, 2) + A_{\beta\gamma, k_x}^*(2) C_{\alpha\gamma, k_x}(1, 2), \quad (5b)$$

$$\partial_a U_a = 0, \quad \hat{\partial}_\alpha(1) C_{\alpha\beta, k_x}(1, 2) = \hat{\partial}_\beta^*(2) C_{\alpha\beta, k_x}(1, 2) = 0, \quad (5c)$$

with summation convention on repeated indices and  $\hat{\partial} \stackrel{\text{def}}{=} (ik_x, \partial_y, \partial_z)$ . In (5b)  $A_{\alpha\beta, k_x}(1)$  [or  $A_{\alpha\beta, k_x}(2)$ ] is the operator governing the linear evolution of streamwise varying perturbations in (1b) with streamwise wave number  $k_x = 2\pi n/L_x$ ,  $n = 1, 2, \dots$ , linearized about the instantaneous streamwise mean flow  $\mathbf{U}(1)$  [or  $\mathbf{U}(2)$ ] and 1 (or 2) indicates that the operator acts on the 1 (or the 2) variable of  $C(1, 2)$ . The subscript 1 = 2 in (5a) indicates that, after differentiation of  $C_{\alpha\beta, k_x}(1, 2)$  with respect to variable 1, the expression is evaluated at the same point. These equations produce at post-transitional Reynolds numbers a transient chaotic trajectory of the S3T SSD state  $(U_\alpha, C_{\alpha\beta, k_x})$ , in which only a small number of streamwise-varying components are sustained corresponding to a small set of wave numbers  $n$ . The time mean of the first two cumulants evolving on the S3T SSD chaotic trajectory are denoted  $\langle \mathbf{U} \rangle_t$  and  $\langle C \rangle_t$ . This time-mean statistical state comprises a mean flow  $\langle \mathbf{U} \rangle_t = (\bar{U}(y), \bar{V}, \bar{W})$ , with  $\bar{V} = \bar{W} = 0$ , which depends only on the cross-stream coordinate, and a second-order cumulant  $\langle C \rangle_t$ , the components of which are homogeneous in the spanwise direction. These cumulant components are also homogeneous in the streamwise direction, as accounted for by allowing the fields to be represented by Fourier decomposition in the streamwise direction.

From (5b) we obtain that the time mean state,  $(\langle \mathbf{U} \rangle_t, \langle C \rangle_t)$  satisfies the equation

$$\bar{A}_{\alpha\gamma, k_x}(1) \bar{C}_{\gamma\beta, k_x}(1, 2) + \bar{A}_{\beta\gamma, k_x}^*(2) \bar{C}_{\alpha\gamma, k_x}(1, 2) = -(\tilde{A}_{\alpha\gamma, k_x}(1) \tilde{C}_{\gamma\beta, k_x}(1, 2) + \tilde{A}_{\beta\gamma, k_x}^*(2) \tilde{C}_{\alpha\gamma, k_x}(1, 2))_t, \quad (6)$$

where  $\bar{C}$  is the time-mean second-order cumulant  $\langle C \rangle_t$ ,  $\bar{A}$  is the operator governing the linear evolution of fluctuations on the time-mean flow  $\bar{U}(y) \hat{\mathbf{x}} \stackrel{\text{def}}{=} \langle \mathbf{U} \rangle_t$ , and tilde denotes the departures from the time mean. We find that the right-hand side (r.h.s.) of (6) does not vanish and consequently  $(\langle \mathbf{U} \rangle_t, \langle C \rangle_t)$  is not a fixed point of the S3T SSD dynamics in post-transitional pCf turbulence. This time-mean state would have been a fixed point of the S3T SSD dynamics if the S3T SSD dynamics had a fixed-point attractor (other than the laminar state), as is often the case in planetary turbulence. Instead, S3T dynamics demonstrates that this time-mean flow is unstable. Identification of this

instability ensures that the ensemble statistical state cannot be associated with a stable flow to which it corresponds, as in the case of beta plane or pretransitional boundary layer time mean states.

We have shown that the ensemble or time mean flow is not sustained by its consistent Reynolds stresses. However, it is a common practice to conjecture the existence of exogenous forces sustaining mean flows. Consistent with this common practice, we can study the S3T SSD stability properties of  $(\langle \mathbf{U} \rangle_t, \langle C \rangle_t)$  by assuming that time-mean stresses sustain these states as equilibria and then determine the stability of these equilibria. This procedure might be realized physically by adding appropriate eddy viscosity to sustain the time-mean velocity as an equilibrium for the sake of studying the hydrodynamic stability properties of a flow, as has been done in the case of the Reynolds-Tiederman turbulent profile [64]. We enforce that  $(\langle \mathbf{U} \rangle_t, \langle C \rangle_t)$  form an equilibrium state by introducing stresses calculated from the simulation so that the SSD equilibrium conditions are satisfied:

$$\Delta \bar{U}_\alpha / \text{Re} + \bar{F}_\alpha = 0, \quad (7a)$$

$$\bar{A}_{\alpha\gamma, k_x}(1) \bar{C}_{\gamma\beta, k_x}(1, 2) + \bar{A}_{\beta\gamma, k_x}^*(2) \bar{C}_{\alpha\gamma, k_x}(1, 2) + \bar{Q}_{\alpha\beta, k_x}(1, 2) = 0, \quad (7b)$$

with both

$$\bar{F}_\alpha = -\frac{1}{2} \sum_{k_x} \Re(\partial_{\beta, 1} \bar{C}_{\alpha\beta, k_x}(1, 2))_{l=2} - \langle \tilde{U}_\beta \partial_\beta \tilde{U}_\alpha \rangle_t + \partial_\alpha \langle P \rangle_t, \quad (8a)$$

$$\bar{Q}_{\alpha\beta, k_x}(1, 2) = \langle \tilde{A}_{\alpha\gamma, k_x}(1) \tilde{C}_{\gamma\beta, k_x}(1, 2) + \tilde{A}_{\beta\gamma, k_x}^*(2) \tilde{C}_{\alpha\gamma, k_x}(1, 2) \rangle_t \quad (8b)$$

obtained from the simulations.

Having obtained in this way an equilibrium of the SSD we can determine its stability by considering the linear evolution of perturbations  $\delta U$  and  $\delta C_{k_x}$  in (5) (cf. Refs. [11, 35]). The perturbation equations that govern the  $(\delta U, \delta C_{k_x})$  about the time-mean state  $(\bar{U}, \bar{C}_{k_x})$  are

$$\partial_t \delta U_\alpha = -\bar{U}_\beta \partial_\beta \delta U_\alpha - \delta U_\beta \partial_\beta \bar{U}_\alpha + \Delta \delta U_\alpha / \Re - \partial_\alpha \delta P - \frac{1}{2} \sum_{k_x} \Re(\partial_{\beta, 1} \delta C_{\alpha\beta, k_x}(1, 2))_{l=2}, \quad (9a)$$

$$\begin{aligned} \partial_t \delta C_{\alpha\beta, k_x}(1, 2) &= \bar{A}_{\alpha\gamma, k_x}(1) \delta C_{\gamma\beta, k_x}(1, 2) + \bar{A}_{\beta\gamma, k_x}^*(2) \delta C_{\alpha\gamma, k_x}(1, 2) \\ &\quad + \underbrace{\delta A_{\alpha\gamma, k_x}(1) \bar{C}_{\gamma\beta, k_x}(1, 2) + \delta A_{\beta\gamma, k_x}^*(2) \bar{C}_{\alpha\gamma, k_x}(1, 2)}_S, \end{aligned} \quad (9b)$$

$$\partial_a \delta U_a = 0, \quad \hat{\partial}_\alpha(1) \delta C_{\alpha\beta, k_x}(1, 2) = \hat{\partial}_\beta^*(2) \delta C_{\alpha\beta, k_x}(1, 2) = 0. \quad (9c)$$

The first equation (9a) governs the evolution of the perturbation of the first cumulant, while (9b) governs those of the second cumulant. The operator  $\bar{A}_{k_x}$  is the operator that governs the evolution of perturbations about the time-mean flow  $\bar{U}$ , and  $\delta A_{k_x}$  denotes the operator that governs the evolution of perturbations about the perturbed streamwise-mean flow  $\delta U$ . The term  $S$  in (9b), which describes the linear interaction between perturbations to the mean flow and the second cumulant of the unperturbed S3T equilibrium state, is responsible for the emergence of the S3T instabilities. When  $\bar{C}_{k_x} = 0$  the first and second cumulant perturbation equations decouple and linear hydrodynamic stability of  $\bar{U}$ , which is determined from eigenanalysis  $\bar{A}_{k_x}$  in (9b), implies the linear S3T stability of the S3T state  $(\bar{U}, 0)$ . In general, the  $k_x$  in (9) are found to span only the small number of streamwise wave numbers that comprise the active subspace sustaining the fluctuations and for which  $\bar{C}_{k_x} \neq 0$ . In the case discussed here the turbulent state is sustained with the single streamwise wave number  $k_x = 2\pi/L_x$ . For the other  $k_x$  that have  $\bar{C}_{k_x} = 0$ , no investigation is necessary as S3T stability is implied from the hydrodynamic stability of the flow.



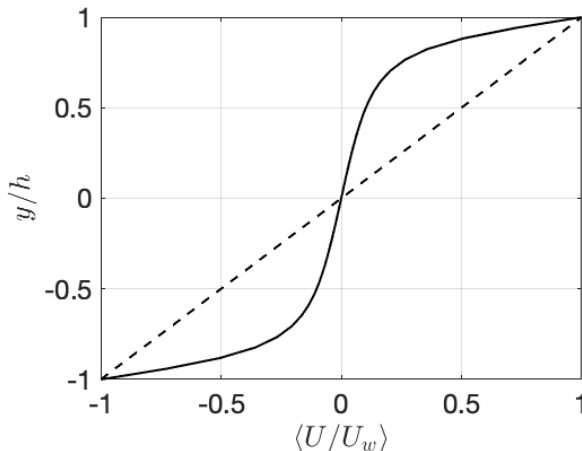


FIG. 1. The mean turbulent velocity profile  $\bar{U}$  in a turbulent RNL simulation of pCf at  $\text{Re} = 600$  in a channel with  $L_x/h = 1.75\pi$  and  $L_z/h = 1.2\pi$ . The shear at the walls is  $4.2U_w/h$ . The laminar Couette flow is shown for comparison (dashed).

### III. RESULTS

We consider a turbulent pCf at  $\text{Re} = 600$  in a channel with  $L_x/h = 1.75\pi$ ,  $L_z/h = 1.2\pi$  in the quasilinear approximation, i.e., neglecting the fluctuation-fluctuation interaction in (1), as discussed in the previous section. The turbulent state supports fluctuations of only the single  $k_x = 2\pi h/L_x$  wave number.

We obtain the flow states for a period of  $10^4 h/U_w$  time units with a discretization on  $N_y = 33$  grid points in  $y$  and  $N_z = 48$  grid points in  $z$ . We have verified that the time period of the simulation is adequate for producing converged results.<sup>1</sup> The time-mean turbulent flow  $\bar{U}(y)$  is shown in Fig. 1, and the structure of two typical fluctuation states are shown in Fig. 2.  $\bar{C}$  is the time-mean covariance of the velocities of the streamwise-varying flow obtained from all the individual snapshots that occur in the simulation. In the process of forming  $\bar{C}$ , the phase information associated with individual fluctuations is lost, while the time-mean Reynolds stresses that balance the time-mean flow are retained. Further insight into the maintenance of the time-mean flow can be obtained from the individual terms contributing to the maintenance. The time-mean flow force balance (7a) for the case of Couette turbulence simplifies to

$$\underbrace{\frac{1}{\text{Re}} \frac{d^2 \bar{U}}{dy^2}}_A - \underbrace{\frac{d\langle u'v' \rangle_x}_t}_{B} - \underbrace{\frac{d\langle \tilde{U}\tilde{V} \rangle_t}_{dy}}_C = 0, \quad (10)$$

with the viscous force (term A), by which the boundaries maintain the flow, being almost exclusively balanced by the time-mean Reynolds stress divergence of the streamwise constant time-varying velocity components (term C) (cf. Fig. 3), consistent with the mechanism of streak displacement by roll circulations in the 2D3C turbulence model of Gayme *et al.* [65]. It is remarkable that the component of the Reynolds stress divergence arising from the streamwise constant flow fluctuations (term C) so dominates the mean velocity force balance. This calls into question the adoption of spatially dependent diffusion as a mechanistic explanation for momentum fluxes maintaining time mean flows insofar as these fluxes are predicated on assuming they arise from small-scale

<sup>1</sup>Convergence to the homogeneous statistical symmetry in wall-bounded flows is very slow. The convergence towards statistical symmetry in pPf is shown in the Appendix of Nikolaidis *et al.* [28].

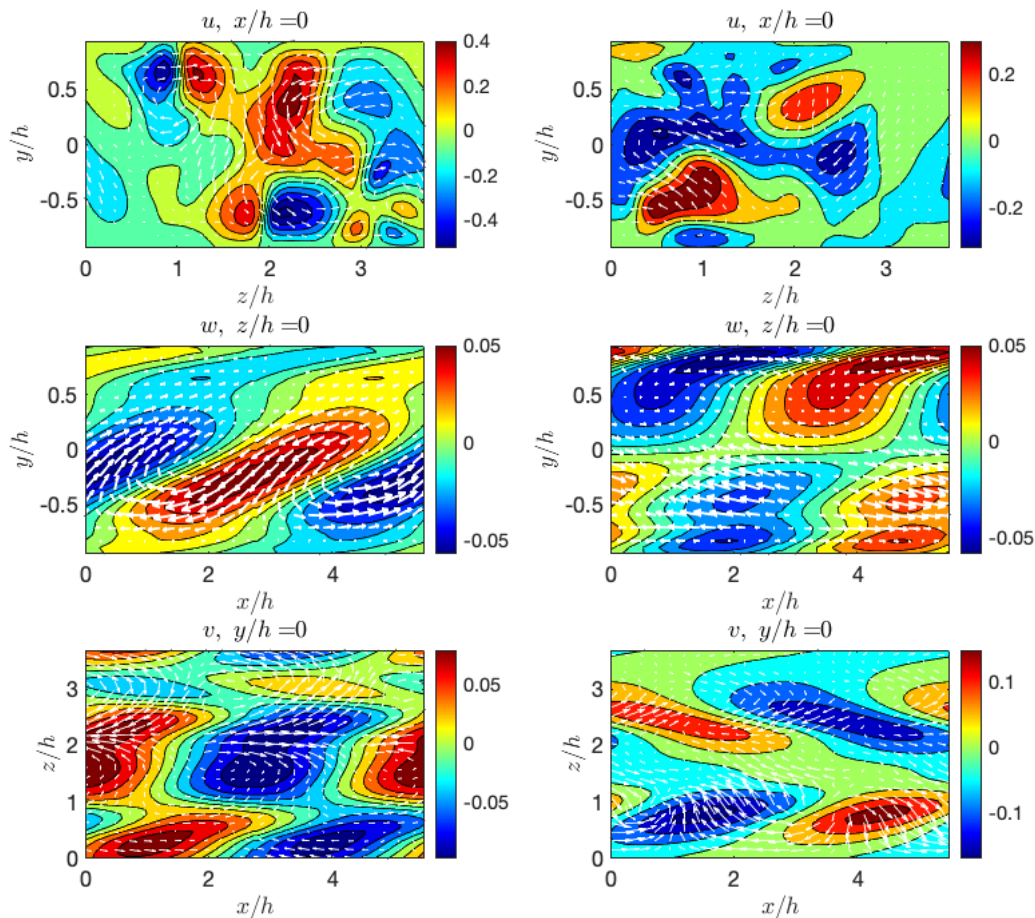


FIG. 2. Columns showing snapshots of the velocity field with  $k_x = 2\pi h/L_x$  for fluctuations of the turbulent flow in an RNL simulation of pCf at  $Re = 600$ . The contour levels indicate the value of the fields. (top row) Contours of  $u'$  velocity and vectors of  $(w', v')$  on the  $x/h = 0$  plane. Maxima of  $(u', v', w')$  are  $(0.46, 0.13, 0.08)$  (left panel) and  $(0.40, 0.21, 0.12)$  (right panel). (middle row) Contours of  $w'$  velocity and vectors of  $(u', v')$  on the  $z/h = 0$  plane. Maxima of  $(u', v', w')$  are  $(0.28, 0.06, 0.10)$  (left panel) and  $(0.20, 0.05, 0.04)$  (right panel). (bottom row) Contours of  $v'$  velocity and vectors of  $(u', w')$  on the center plane,  $y/h = 0$ . Maxima of  $(u', v', w')$  are  $(0.34, 0.22, 0.10)$  (left panel) and  $(0.27, 0.24, 0.17)$  (right panel). Note that while the Reynolds stresses arising from averaging over these states are retained in  $\bar{C}$ , the phases determining the exact structures are not retained.

velocity correlations. The stress divergence arising from the time-mean eddy Reynolds stress of the streamwise varying components, obtained from the covariance  $\bar{C}$  (term B), makes a minor contribution to the force balance (10).

While  $\bar{C}$  is by necessity positive definite, being the time average of the instantaneous positive-definite covariances of the fluctuations, this is not guaranteed for the time-mean  $\bar{Q}$  obtained in (8b). We find that  $\bar{Q}$  is nonpositive definite, as was also found by Zare *et al.* [49] in a DNS of wall-bounded turbulence. This implies that if  $\bar{Q}$  were to represent the spatial covariance of a stochastic excitation, this stochastic excitation must be temporally correlated (colored) [49].

The operator  $\bar{A}_{k_x}$  in (7b) governing the evolution of perturbations about the time-mean flow  $\langle \mathbf{U} \rangle_t \stackrel{\text{def}}{=} \bar{U}(y)$  is stable by the least damped mode at streamwise wave number  $k_x = 2\pi h/L_x$  decaying rate  $\sigma = -0.11U_w/h$ . As is the case for the Reynolds-Tiederman mean-flow, the time-

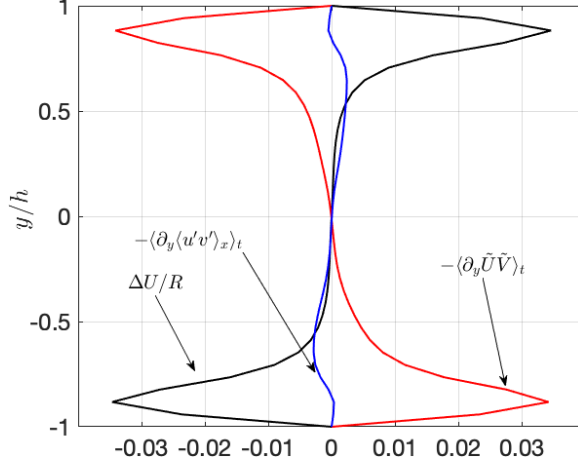


FIG. 3. The force balance of the time-mean flow in pCf at  $\text{Re} = 600$ . The viscous force  $\text{Re}^{-1}d\bar{U}/dy^2$  is primarily balanced by the divergence of the time mean Reynolds stress of the fluctuations of the streamwise-mean flow  $-\langle\partial_y\langle\bar{U}\bar{V}\rangle_x\rangle_t$ . The divergence of the Reynolds stress of the streamwise-varying fluctuations,  $-\langle\partial_y\langle u'v'\rangle_x\rangle_t$  is small.

mean turbulent pCf flow  $\bar{U}(y)$  is far from a state of marginal hydrodynamic stability, violating the conjecture of Malkus that the time-mean flow is adjusted by turbulence to neutral stability, as occurs in Rayleigh-Bénard convection [64,66]. However, here we show that the time-mean flow, although hydrodynamically stable, is unstable to the nonlinear instability revealed by the S3T dynamics.

To proceed with the S3T stability analysis of the turbulent state ( $\langle\mathbf{U}\rangle_t$ ,  $\langle C\rangle_t$ ) we consider the stability of equations (9) governing cumulant perturbations about ( $\langle\mathbf{U}\rangle_t$ ,  $\langle C\rangle_t$ ). The discretized linear operator that governs perturbations  $(\delta U, \delta V, \delta W, \delta C_k)$  in (9) has dimensionality  $2N_y N_z(2N_y N_z + 1) \times 2N_y N_z(2N_y N_z + 1)$ , which is  $\approx 10^7 \times 10^7$  in the model example we study, necessitating the use of the power method to obtain the fastest growing eigenvalues and eigenmodes of the equilibrium state ( $\langle\mathbf{U}\rangle_t$ ,  $\langle C\rangle_t$ ), as discussed in Refs. [11,12]. Due to the spanwise homogeneity of the background state, the perturbation eigenmodes are harmonic in  $z$  with mean flow components  $(\delta U_m(y), \delta V_m(y), \delta W_m(y))e^{imz}$ , where  $m$  is the spanwise wave number, with corresponding covariance  $\delta C_{m,k_x}(y_1, y_2)e^{im(z_1 - z_2)}$ . The growth rates of the most unstable S3T symmetric and antisymmetric in  $y$  eigenfunctions as a function of  $m$  are shown in Fig. 4. While the spanwise constant perturbations ( $m = 0$ ) are S3T stable with structure shown in Fig. 5, the introduction of spanwise variation results in the time-mean flow being unstable to  $m = 1\beta, 2\beta, 3\beta$  S3T perturbations, with  $\beta = 2\pi h/L_z$  the fundamental spanwise wave number. The  $(\delta U_m(y), \delta V_m(y), \delta W_m(y))e^{imz}$ , component of the two most unstable eigenmodes of the perturbation S3T dynamics, with  $m = 2\beta$  and  $m = 3\beta$ , are shown in Fig. 6. These unstable eigenmodes have the form of streamwise roll-streak (R-S) structures. This is also the case for the S3T eigenmodes of the laminar profile, but in contrast with the laminar flow S3T eigenmodes these R-S structures are confined to the near-wall, high-shear regions of the mean turbulent profile. This universality of the structure of the S3T eigenfunctions reflects the universality in the mechanism of the S3T R-S instability [11,67]. The two most unstable eigenmodes have real eigenvalues with growth rates  $\sigma = 0.04U_w/h$  and  $\sigma = 0.034U_w/h$  for spanwise wave number  $m = 2\beta$  and  $m = 3\beta$ , respectively. Both eigenmodes are antisymmetric in  $y$ . Their symmetric counterpart eigenmodes are also unstable but with the smaller growth rates  $\sigma = 0.025U_w/h$  and  $\sigma = 0.032U_w/h$ , respectively. As shown in Fig. 4, degeneracy of the growth rates between the symmetric and antisymmetric in  $y$  modes is approached as  $m$  increases. Degeneracy is expected as the velocity fields associated with the modes become more confined to their respective boundaries with either increase in  $m$  or  $\text{Re}$ .

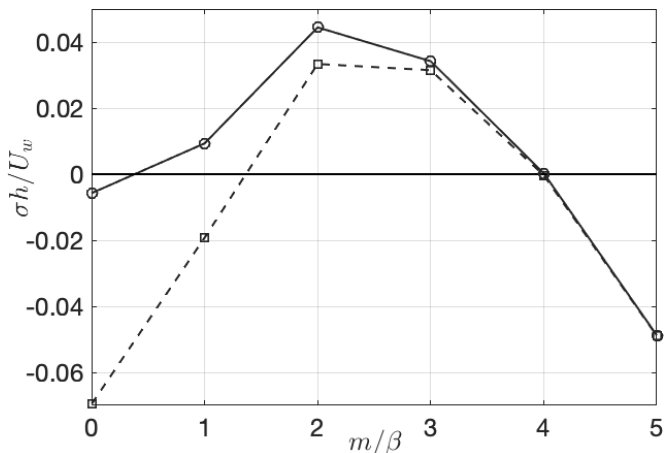


FIG. 4. Growth rates of the most unstable S3T eigenmodes of the turbulent time-mean pCf mean flow shown in Fig. 1 as a function of the order of the spanwise harmonic,  $m/\beta$ , with  $\beta = 2\pi h/L_z$  being the fundamental spanwise wave number. The solid line shows growth rates of the antisymmetric-in- $y$  eigenfunctions. The dashed line shows growth rates of the symmetric-in- $y$  eigenfunctions.

We conclude that the S3T SSD equilibrium state in pCf is unstable to perturbations with R-S structure and therefore cannot be used to obtain the linear dynamics of perturbations from the mean statistical state by performing a perturbation analysis of the S3T SSD about the mean turbulent state. We note that the R-S unstable modes in turbulent flows depend only on the shear and similar unstable structures are expected to be found in other wall-bounded flows such as pPf and boundary layers. The fact that an ensemble mean state can be stable in ensemble dynamics while the same state is a repeller can be understood by recalling the example of a mass-spring with random restoring

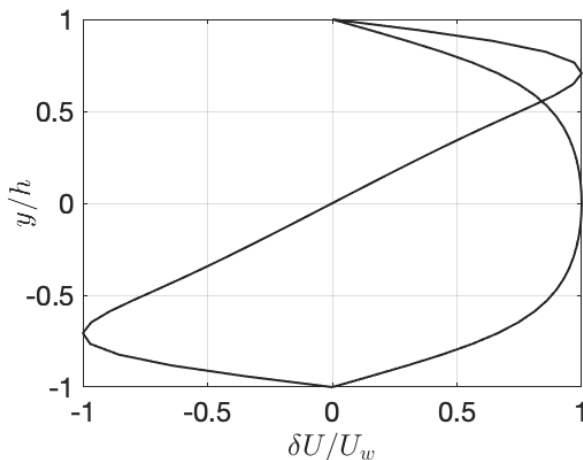


FIG. 5. The structure of the  $\delta U$  component of the first two least stable S3T spanwise constant ( $m = 0$ ) eigenmodes of the turbulent pCf, for which  $\delta V = \delta W = 0$ . The time-mean flow when maintained to be a S3T equilibrium is stable to  $m = 0$  (spanwise constant) but unstable to spanwise varying perturbations, as shown in Fig. 4. The antisymmetric perturbation is the least stable with decay rate  $\sigma = -0.006U_w/h$  while the least stable symmetric perturbation has decay rate  $\sigma = -0.07U_w/h$ . These stable  $m = 0$  modes do not correspond to the least stable eigenfunctions of the dynamics of relaxation to the time-mean flow, which are shown in Fig. 8.

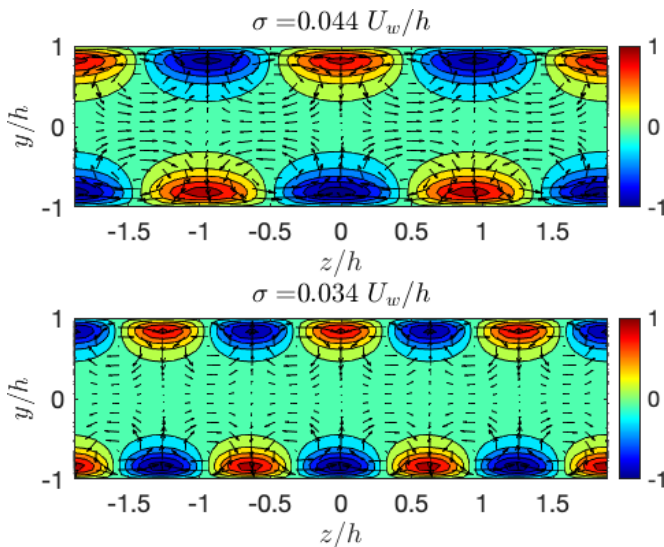


FIG. 6. The structure of the first two most unstable eigenmodes of the turbulent pCf mean flow shown in Fig. 1 obtained by eigenanalysis of the operator governing the evolution of perturbations in the S3T equations. The most unstable eigenmode with spanwise wave number  $m = 2\beta$  (top panel) has growth rate  $\sigma = 0.044U_w/h$ , while the second most unstable eigenmode with  $m = 3\beta$  (bottom panel) has growth rate  $\sigma = 0.034U_w/h$ . The first cumulant component of the S3T eigenfunction has roll-streak structure. Shown are contours of the streamwise mean velocity,  $\delta U$  (the contour level spacing is 0.2), and velocity vectors of the components ( $\delta V$ ,  $\delta W$ ) on the  $(y/h, z/h)$  plane. Consistent with the lift-up mechanism, positive  $\delta V$  is associated with negative  $\delta U$ . The maxima of  $(\delta U, \delta V, \delta W)$  are proportional to  $(1, 0.23, 0.26)$  in the  $m = 2\beta$  S3T eigenfunction and proportional to  $(1, 0.25, 0.22)$  in the  $m = 3\beta$  S3T eigenfunction.

force governed by the Mathieu equation [23]. Each realization of the state is unstable while the ensemble mean evolves as a stable harmonic oscillator with the average square frequency of the ensemble realizations. This example shows how the time-mean state may be an attractor for the ensemble mean but at the same time be a repeller for the perturbation dynamics, as is the case for wall turbulence.

#### IV. EMPIRICAL DETERMINATION OF THE EFFECTIVE LINEAR DYNAMICS OF PERTURBATIONS TO THE TIME-MEAN EQUILIBRIUM STATE IN A TURBULENT CHANNEL FLOW

Perturbation analysis of the S3T SSD equilibrium state provides comprehensive characterization of turbulent state stability in cases for which a stable S3T SSD equilibrium state exists. However, turbulent pCf and pPf lie on a transient chaotic attractor in statistical state space. Stability of the ensemble mean (or equivalently the time-mean) statistical state in these cases requires obtaining the perturbation dynamics averaged over the chaotic attractor. This can be accomplished by restricting attention to the time-mean flow component of the statistical state. As discussed in the introduction, IWCV found these first two eigenmodes and eigenvalues by averaging an ensemble of pPf DNS runs at  $\text{Re}_\tau = 180$  in a channel with  $L_x/h = 8\pi$  and  $L_z/h = 4\pi$ ,  $L_y/h = 2$ , which had been perturbed by the same initial streamwise flow perturbation  $\delta U(y)$ . Here we obtain an approximate dynamical system in Langevin form for the relaxation of mean flow perturbations to the time mean using an alternative method, called linear inverse modeling. Linear inverse modeling (LIM) obtains the effective dynamics of perturbations to the time-mean flow by observing the behavior of fluctuations to the time-mean velocity profile naturally occurring in the turbulence. In our study we first obtain using

LIM the empirical dynamical system that governs the fluctuations from the streamwise-spanwise mean flow in the pCf simulation presented in the previous section, sampled every nondimensional time unit, which we verified to adequately sample the temporal fluctuations of the streamwise and spanwise mean flow and also in a pPf at  $Re_\tau = 180$  in a channel of  $L_x/h = 2\pi$  and  $L_z/h = \pi$ ,  $L_y/h = 2$ , with bulk velocity,  $U_b$ . The pPf data were obtained using a constant mass-flux DNS. The pPf and the pCf were integrated over a sufficient time ( $6 \times 10^4 h/U_b$  for the pPf and  $10^4 h/U_w$  for the pCf) to obtain converged results as verified by using the data for half the interval.

From the data we obtain the time series of the fluctuations  $\delta U(y, t)$  about the time-mean flow with the asymptotic statistical symmetry of the time-mean flow,  $\bar{U}(y)$ , about the center-plane in the cross-flow direction in pPf and antisymmetry in pCf enforced by adding replicas of the mirror symmetric instantaneous mean flows about the center-plane in pPf and mirror antisymmetric replicas in pCf. Although the instantaneous realizations of the streamwise-spanwise averaged flow are not symmetrized, this symmetrizing operation results in the time-mean flow obtained from our finite dataset, as well as in the time-mean statistical moments of the fluctuations to be exactly symmetric in pPf and antisymmetric in pCf. An important consequence of this symmetrization procedure is that it enforces in the data the known symmetries of the dynamics of pCf and pPf.

From the  $\delta U(y, t)$  fluctuations we also obtain the time-mean fluctuation covariance:

$$C_0(1, 2) = \langle \delta U(y_1, t) \delta U(y_2, t) \rangle_t, \quad (11)$$

and the time-mean time-lagged covariances:

$$C_\tau(1, 2) = \langle \delta U(y_1, t + \tau) \delta U(y_2, t) \rangle_t. \quad (12)$$

Due to the mean flow symmetrization procedure, the covariance  $C_0$  and  $C_\tau$  are symmetric about the  $x$ - $z$  plane at the channel center, i.e., they satisfy  $C(y_1, y_2) = C(y_1^s, y_2^s)$ , where  $y_i^s$ ,  $i = 1, 2$ , is the symmetric coordinate of  $y_i$  with respect to the channel center. The proper orthogonal decomposition (POD) modes of the mean flow fluctuations are obtained from the eigenanalysis of  $C_0$ . Due to the statistical symmetry reflected in  $C_0$ , the POD modes are necessarily either symmetric or antisymmetric.

LIM determines the best fit to our data by the linear stochastic system with Langevin form:

$$\frac{d\delta U}{dt} = A\delta U + \xi(t), \quad (13)$$

where  $\delta U$  is the column vector of the values at the  $N_y$  wall-normal grid points,  $A$  is the  $N_y \times N_y$  matrix generator of the dynamics of fluctuations, and  $\xi(t)$  represents the spatial and temporal structure of the unresolved dynamics that are required to be parametrized as a zero mean temporally delta correlated Gaussian noise process satisfying  $\langle \xi(y_1, t) \xi(y_2, t') \rangle_E = \Xi(1, 2) \delta(t - t')$ , with the full rank positive-definite spatial covariance  $\Xi(1, 2)$  to be determined, along with the effective linear operator  $A$ , by inversion for the best fit to the dynamics (13). Note that LIM does not determine  $\xi$ , it determines only its spatial covariance  $\Xi$ . In LIM the operator  $A$  is discovered and is not assumed *a priori* to be either the operator  $\bar{A}$  that governs perturbations about the mean flow,  $\bar{U}$ , or  $\bar{A}$  modified by eddy viscosity as in the studies of Hwang and Eckhardt [30], Zare *et al.* [49], Towne *et al.* [50], Holford *et al.* [53], Holford and Hwang [54], and Abootorabi and Zare [55].

With a discretized representation the time lagged covariances of the velocity fluctuations,  $C_0$  and  $C_\tau$  in (11) and (12) become matrices. Under the assumption that the stochastic excitation  $\xi$  in (13) is temporally white it can be shown (cf. Ref. [41]) that

$$C_\tau = e^{A\tau} C_0, \quad \tau > 0, \quad (14)$$

from which we obtain immediately that

$$A = \frac{1}{\tau} \ln(C_\tau C_0^{-1}). \quad (15)$$

The logarithm of any matrix  $M$  that has a full basis of eigenvectors is  $\log(M) = UDU^{-1}$ , where  $U$  is the matrix of the eigenvectors of  $M$  and  $D$  the diagonal matrix with diagonal elements the logarithms of the eigenvalues of  $M$ .

If there is an interval in  $\tau$  for which  $\tau$  is both small enough to sample the dynamics and large enough that the correlation time of the fluctuations perturbing the eigenmodes can be represented by a Gaussian delta-correlated white-noise process, so that in this interval  $A$  is insensitive to  $\tau$ , then  $A$  identifies the generator of the Langevin dynamics (13) rather than being merely the finite time map connecting  $C_0$  to  $C_\tau$  [40,68–70].

Boundedness of  $C_0$  ensures the stability of the matrix  $A$  and (13) requires that the covariance of the noise process  $\Xi$  satisfies the Lyapunov equation:

$$AC_0 + C_0A^T = -\Xi. \quad (16)$$

$\Xi$  must be verified for consistency to be positive semidefinite given that it is the correlation of the forcing vector structures [40]. In this way LIM identifies the linear operator  $A$  that best fits the data while also determining the positive semidefinite spatial covariance  $\Xi$  of the effectively white temporal excitation of the fluctuations. By contrast, note that Zare *et al.* [49] constrain their stochastic model operator to be  $\bar{A}$ , which governs perturbations about the time-mean flow  $\bar{U}$ . The consequence is that the  $\Xi$  that is obtained using (16) may not be positive definite. Such a nonpositive  $\Xi$  is compatible with a set of stochastic models excited by colored noise [49,71]. To remove ambiguity among the members of this set Zare *et al.* [49] employ an optimization procedure. Moreover, Georgiou [71], Zare *et al.* [72], and Zare *et al.* [49] show that each of these colored noise models with linear operator  $A_{col}$  corresponds to a linear model with an appropriately modified operator  $A_{white}$  driven by a white-noise process. Importantly, the LIM removes the ambiguity in the choice of  $A_{white}$  by determining the operator that best fits the data. LIM determines a unique operator by using the extra information encoded in the time lagged covariances, while Zare *et al.* [49] utilize only the information encoded in  $C_0$ . A clue to the underlying importance of identifying the unique LIM modified operator  $A$  is offered in DelSole and Farrell [45] who show that the modified  $A$  in two-layer baroclinic turbulence model is the linear operator about the time mean flow,  $\bar{A}$ , corrected by the addition of a diffusion operator. This is consistent with the works of Hwang and Eckhardt [30], Holford *et al.* [53], Holford and Hwang [54], and Abootorabi and Zare [55] who match the observed covariances by forcing white the linear operator about the mean flow,  $\bar{A}$ , modified by the inclusion of a diffusive operator with the Reynolds-Tiederman diffusion coefficient, indicating that the color of the stochastic forcing can be compensated for by inclusion of a parametrization of eddy viscosity in the form of a spatially varying diffusion. However, LIM allows going a step further by obtaining the unique form of this diffusion and by so doing providing an independent justification for the use of eddy diffusion as a parametrization of unresolved scales in turbulence models.

Another consideration for obtaining the effective dynamics is that the inverse of  $C_0$  is ill-conditioned for data from a turbulent flow given that any finite time series cannot resolve fluctuations of arbitrarily small scale and amplitude (cf. North *et al.* [73]). Therefore, in order to obtain a converged dynamics we confine the representation of the dynamics to the subspace spanned by a set of dominant POD modes obtained from the covariance  $C_0$  of the  $\delta U$  fluctuations.

We first obtain the effective  $2 \times 2$  dynamical operator  $A$  governing the dynamics of the fluctuations to the time-mean flow in the space of the top 2 POD modes in the pCf S3T and the pPf DNS, which account for  $\approx 70\%$  and  $\approx 40\%$  of the energy, respectively. The top two POD modes are a symmetric and antisymmetric pair with structure shown in Fig. 7. We obtain the operator  $A$  from (15) and verify that the noise covariance  $\Xi$  from (16) is positive definite. Insensitivity of the dynamics was obtained for time-lags around  $\tau U_b/h = 18$  in both pCf and pPf. The eigenmodes of  $A$  are found to have the same structure as the POD modes used in the projection. The eigenvalue of the least damped antisymmetric mode is  $\sigma = -0.03U_b/h$  and that of the symmetric mode is  $\sigma = -0.05U_b/h$ . The least damped eigenmode, shown in the top-left panel of Fig. 8, is antisymmetric with respect to the channel center, consistent with the results of IWCV. However, our LIM analysis predicts a

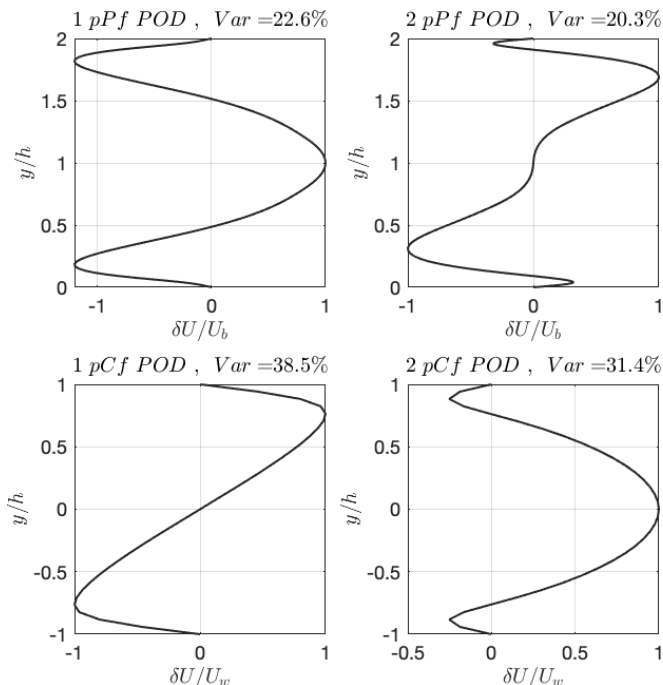


FIG. 7. The structure of the first two POD modes of the mean flow fluctuations in pPf (top), and in pCf (bottom). (top-left panel) The first POD mode of pPf accounts for 23% of the energy of the fluctuations. (top-right panel) The second POD of pCf accounts for 20% of the energy of the fluctuations. (bottom-left panel) The first POD mode of pCf accounts for 39% of the energy of the fluctuations. (bottom-right panel) The second POD of pCf accounts for 31% of the energy of the fluctuations.

slower decay rate than theirs. The next in decay rate mode of  $A$ , shown in the top-right panel of Fig. 8, is symmetric and its decay rate and structure are consistent with the least damped symmetric eigenmode of IWCV. The least damped eigenmodes in pCf are also real as shown in the lower panels of Fig. 8. The eigenvalue of the symmetric mode is  $\sigma = -0.02U_w/h$ , and that of the asymmetric mode is  $\sigma = -0.06U_w/h$ . While the POD modes have the same structure as the eigenmodes of  $A$ , in pPf the least damped antisymmetric mode of  $A$  is excited less vigorously by  $\Xi$ , with the result that the dominant POD becomes the symmetric, although this is the more damped eigenmode of  $A$ . Similarly, in pCf the antisymmetric mode is favored by the excitation so that it accumulates more energy in the mean than does the least damped symmetric mode.

Coincidence of the modes of  $A$  with the orthogonal POD modes imply the normality of  $A$ . Note that reflection symmetry of the ensemble dynamics about the cross-stream channel center requires that symmetric structures in the ensemble dynamics evolve to symmetric structures and antisymmetric to antisymmetric. Consequently, in the linear dynamics of the ensemble the eigenmodes of the dynamics are partitioned into a mutually orthogonal symmetric and antisymmetric set and the covariance of the excitation does not mix the symmetric and antisymmetric subspaces. An example of this property is the diagonal structure of both  $A$  and of the spatial covariance  $\Xi$  in the  $2 \times 2$  projection of the dynamics. From this observation we also understand that any non-normality which may arise at higher truncations will be limited to the respective symmetric and antisymmetric subspaces (cf. the Appendix for a discussion of the case of a  $6 \times 6$  truncation).

Given the constraints on the dynamics arising from projections onto a single symmetric and a single antisymmetric POD mode, we consider higher-order truncations. As already discussed, non-orthogonality can only emerge among the antisymmetric (or symmetric) eigenmodes of  $A$  and other



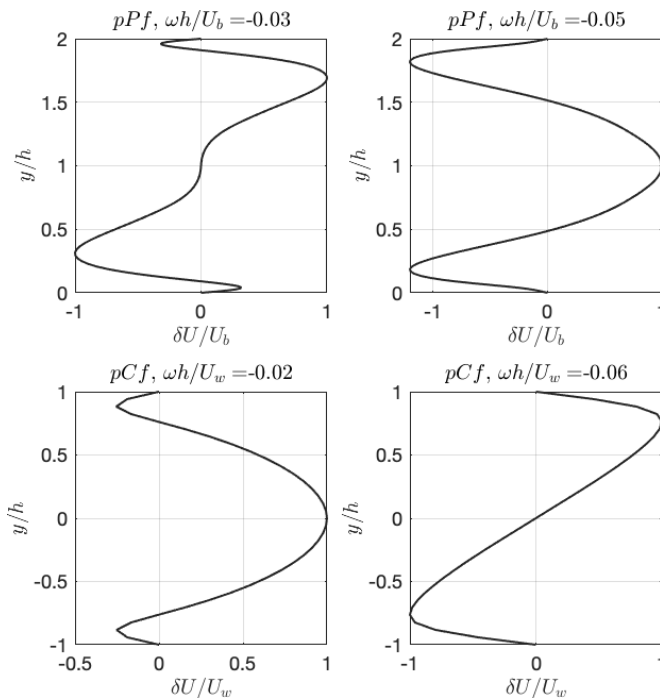


FIG. 8. Structure of the eigenmodes of the  $2 \times 2$  LIM operator governing the relaxation of steamwise and spanwise mean flow fluctuations to the time-mean flow. (top-left panel) The least damped mode in pPf is antisymmetric about the channel center and has eigenvalue  $\omega h/U_b = -0.03$ . (top-right panel) The second least damped mode is symmetric and has eigenvalue  $\omega h/U_b = -0.05$ . (bottom-left panel) The least damped mode in pCf is symmetric about the channel center and has eigenvalue  $\omega h/U_w = -0.02$ . (bottom-right panel) The second least damped mode is antisymmetric about the channel center and has eigenvalue  $\omega h/U_b = -0.06$ .

antisymmetric (or symmetric) eigenmodes of  $A$ . We demonstrate the emergence of non-normality in the dynamics in the case of the pPf by retaining in the dynamics the first six POD modes, which together account for 90% of the mean-flow fluctuation energy. The results that we present do not appreciably change when the dimension of the retained POD modes is increased to 10. With six POD modes we find that  $\tau = 18h/U_b$  produces a  $\tau$ -insensitive dynamical operator  $A_6$  and converged positive-definite covariance,  $\Xi$  (cf. the Appendix for details). We conclude that, in pPf, the dynamics of perturbations to the time mean flow is generated by the matrix  $A_6$  the eigenvalues of which are  $-0.02U_b/h$ ,  $-0.04U_b/h$ ,  $(-0.07 \pm 0.05i)U_b/h$ ,  $(-0.14 \pm 0.06i)U_b/h$ . The least damped eigenmode, shown in the top-left panel of Fig. 9, is antisymmetric with respect to the channel center, consistent with the results of IWCV. However, our LIM analysis predicts a slower decay rate than theirs for the same  $Re_\tau$ , albeit in a channel of one-fourth size. The next in decay rate mode of  $A_6$  is symmetric in structure with decay rate and structure consistent with the real part of the least damped symmetric eigenmode of IWCV. Although the first two eigenvalues of  $A_6$  are real and represent the ensemble mean relaxation of structures of fixed form to the mean flow with timescales of  $\approx 50h/U_b$  and  $\approx 25h/U_b$  respectively, the remaining eigenmodes represent a damped oscillatory relaxation to the mean flow which oscillates between the real part and the imaginary part of the eigenmode over  $\approx 100h/U_b$ , which is the characteristic period of the SSP cycle [36]. The evolution of the oscillating structure of the two complex eigenmodes is shown in Fig. 10.

The operator  $A_6$  governing the dynamics is non-normal in the energy norm, as was conjectured by IWCV. The inner product of the eigenmodes shows that there are substantial projections among modes in both the symmetric and antisymmetric subspace and therefore the operator  $A_6$  is substan-

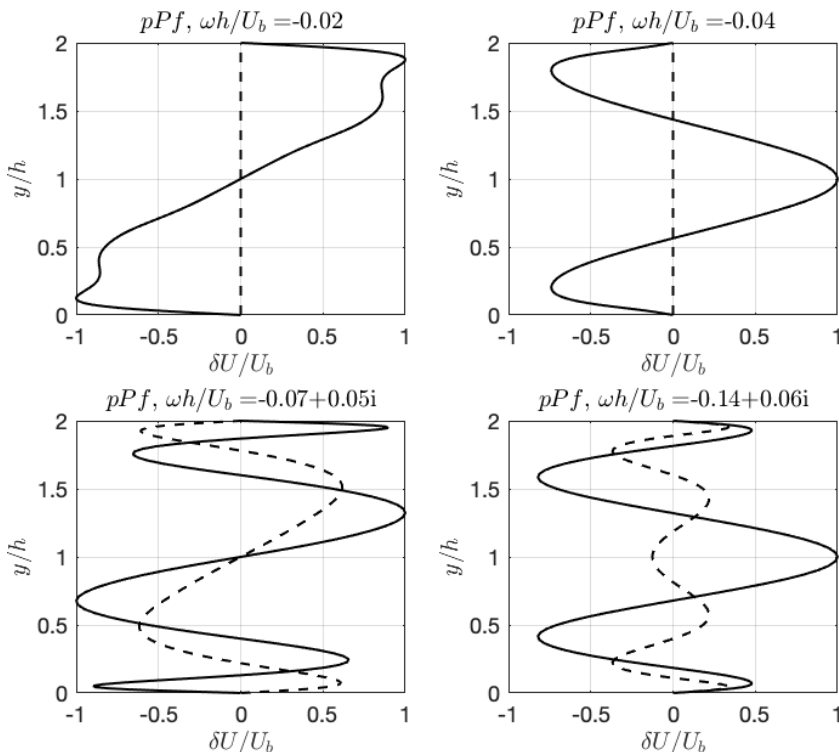


FIG. 9. The structure of the real part (solid line) and the imaginary part (dashed line) of the six damped eigenmodes of the empirical operator  $A_6$  of the pPf. (top-left panel) The least damped mode is antisymmetric about the channel center and has eigenvalue  $\omega h/U_b = -0.02$ . (top-right panel) The next least damped mode is symmetric and has eigenvalue  $\omega h/U_b = -0.04$ . (bottom-left panel) The third and fourth least damped modes are antisymmetric about the channel center and have eigenvalues  $\omega h/U_b = -0.07 \pm 0.05i$ . (bottom-right panel) The fifth and sixth least damped modes are symmetric about the channel center and have eigenvalues  $\omega h/U_b = -0.14 \pm 0.06i$ . The structure of the complex-valued eigenmodes periodically vary with a period of  $T = O(100)h/U_b$ .

tially non-normal (cf. the Appendix). The difference in structure between the eigenmodes and the POD modes reflects both the degree of non-normality of  $A_6$  and the degree of noncommutation of  $A_6$  with the excitation covariance  $\Xi_6$  [74,75]; in general, the POD modes in this Langevin system coincide with the eigenmodes of the linear operator  $A$  when  $A$  is normal and  $[A, \Xi] = 0$  (see the Appendix). Figure 11 shows that the structure of the eigenmodes departs appreciably from that of the associated POD modes. Moreover, non-normality of the dynamics is not consistent with a strictly diffusive process. However, it could be argued that the flow relaxes through the smoothing that results from the advection induced by the random action of the streamwise roll motions over the ensemble realizations of the flow and therefore the dynamics might be modeled as a diffusion with an appropriate coefficient assuming diffusion to be broadly conceived as any transport process resulting in a linear flux or gradient relation. To evaluate this hypothesis we compare the decay rates and structures of the eigenmodes predicted by an eddy viscosity model in which the mean flow perturbations are governed by

$$\frac{\partial \delta U}{\partial t} = \frac{\partial}{\partial y} \left( \nu_E(y) \frac{\partial \delta U}{\partial y} \right), \quad (17)$$

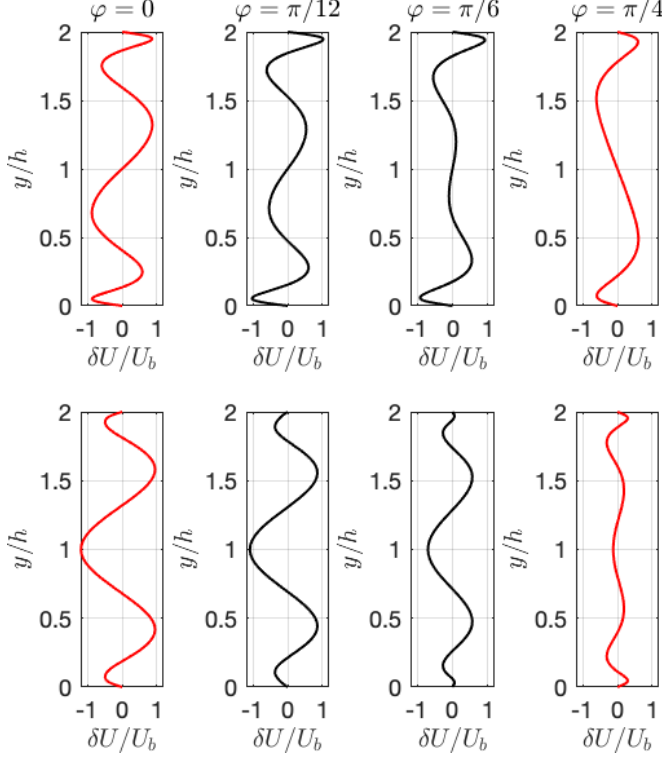


FIG. 10. Evolution of the structure of the complex eigenmodes of  $A_6$  over a quarter period of their oscillation. The decay is not included in this representation. (top panels) For the antisymmetric eigenmode shown in Fig. 9(c) with period  $125h/U_b$ . (bottom panels) For the symmetric eigenmode in Fig. 9(d) with period  $105h/U_b$ .

with  $v_e(y)$  an eddy viscosity coefficient. We obtain the eigenvalues and eigenmodes in the case of simple diffusion with  $v_e(y) = 1/\text{Re}$ , with  $\text{Re}$  the laminar value of the Reynolds number, and the eddy viscosity that sustains the Reynolds-Tiederman [64] turbulent profile in a pPf channel with walls at  $y = 0$  and  $y = 2$ . This profile is maintained by  $v_E = [1 + E(y)]/\text{Re}_\tau$  and  $E(y) = [(1 + e^2)^{1/2} - 1]/2$ , where

$$e(y) = \frac{k\text{Re}_\tau}{3} [1 - (y - 1)^2] \{1 + 2(y - 1)^2\} \{1 - \exp[-\text{Re}_\tau(1 - |y - 1|)/A]\}, \quad (18)$$

with  $K = 0.525$  and  $A = 37$ , as is appropriate for  $\text{Re}_\tau = 180$ . The least damped modes comprise a symmetric and antisymmetric pair, shown in Fig. 11. These modes are qualitatively similar to the modes obtained by LIM (cf. Fig. 11), but lack the detailed structure of the LIM or IWCV eigenmodes. Also, the decay rates of the two least damped modes are underpredicted by a factor  $O(10)$  in the case of the molecular viscosity parametrization, and overpredicted by a factor of  $O(10)$  in the case of the eddy viscosity parametrization that produces the Reynolds-Tiederman turbulent mean flow. These results suggest caution in interpreting the eddy viscosity required to produce the observed mean flow to be an equivalent diffusion that is at the same time acting on smaller scale structures. This is consistent with the findings of Russo and Luchini [76].

LIM not only predicts the decay rate of perturbations to the time-mean flow but also predicts the variance of the perturbations around the decaying trajectory. The Langevin dynamics of the fluctuations obtained using LIM predicts a slight non-normal modification of the exponential decay

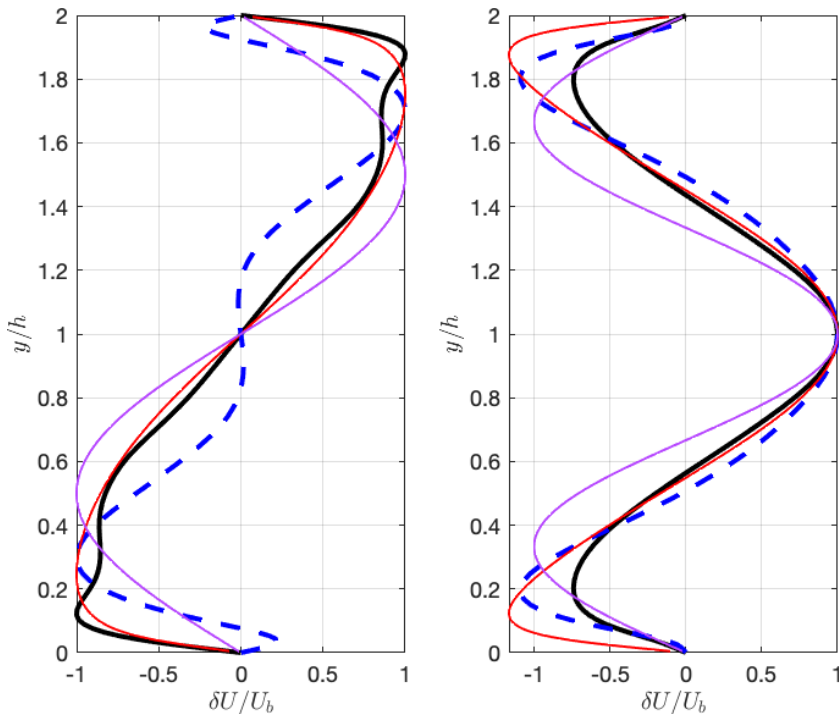


FIG. 11. Comparison of the structure of the antisymmetric (left panel) and symmetric (right panel) least damped mode of  $A_6$  (black line) and of the corresponding modes in diffusive models. Red lines show the least decaying modes of the Reynolds-Tiederman eddy-viscosity model at  $\text{Re}_\tau = 180$  (red). Purple solid lines show the least damped modes of the purely diffusive model with  $\text{Re} = 2767$ , corresponding to the laminar Reynolds number associated with  $\text{Re}_\tau = 180$ . The structure of the top POD modes is indicated with the dashed blue line. The departure of the  $A_6$  modes from the associated POD mode indicates the degree of non-normality of the ensemble dynamics of relaxation to the mean and the degree of noncommutation of  $A_6$  with  $\Xi_6$ .

of the modes to the time-mean opposed by diffusive spreading of the modes away from the time-mean produced by the stochastic forcing. The resulting PDF for the case of the  $2 \times 2$  dynamics obtained by LIM, which is normal implying no mode coupling, can be obtained from the companion Fokker-Planck equation:

$$\frac{\partial f}{\partial t} = -\omega \frac{\partial(xf)}{\partial x} + D \frac{\partial^2 f}{\partial x^2}, \quad (19)$$

in which  $f$  is the perturbed mode probability distribution,  $x$  is the value of the coefficient of the projection on the associated POD mode, and  $D$  is the diffusion coefficient equal to half the corresponding diagonal element of the covariance  $\Xi$  that excites the associated eigenmode of  $A$  with a stable, real eigenvalue  $\omega$ .<sup>2</sup> The perturbed mode distribution drifts back to the equilibrium under the influence of  $\omega$  around which it maintains the predicted asymptotic distribution:

$$f(x) = \frac{\sqrt{-\omega}}{\sqrt{2\pi D}} \exp\left(\frac{\omega}{2D}x^2\right) \quad (\omega < 0). \quad (20)$$

<sup>2</sup>In pPf:  $D = 1.8e - 06$  for the symmetric mode with  $\omega = -0.05$  and  $D = 0.85e - 06$  for the antisymmetric mode with  $\omega = -0.03$ . In pCf  $D = 0.6e - 03$  for the symmetric mode with  $\omega = -0.02$  and  $D = 1.85e - 03$  for the antisymmetric mode with  $\omega = -0.06$ .

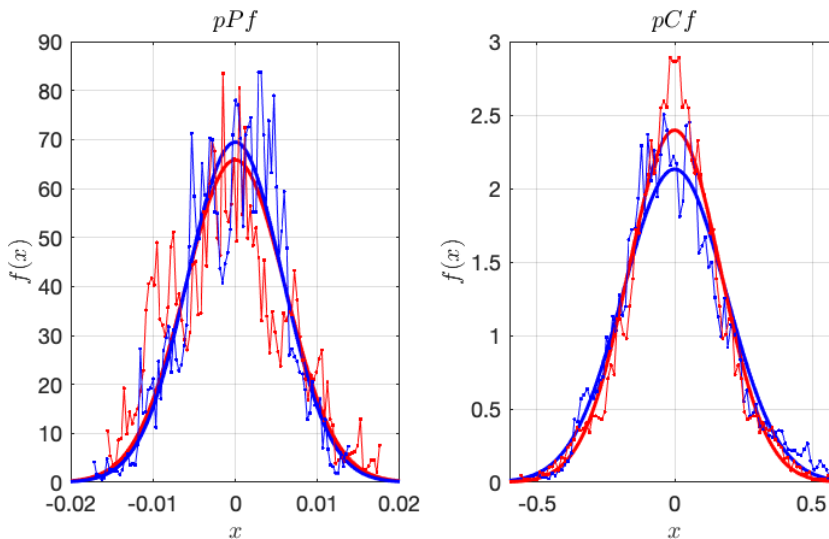


FIG. 12. Comparison between the LIM prediction and the observed PDF of fluctuations. The predicted PDF was obtained from the  $2 \times 2$  LIM. (left panel) For the pPf shown separately are the probability of projection on the symmetric POD (red) and the antisymmetric POD (blue). The symmetric mode has  $\omega = -0.05$  and  $D = 1.8e - 06$  and the antisymmetric has  $\omega = -0.03$  and  $D = 0.85e - 06$ . (right panel) For the pCf, the symmetric mode has  $\omega = -0.02$  and  $D = 0.6e - 03$  and the antisymmetric mode has  $\omega = -0.06$  and  $D = 1.85e - 03$ .

The probability distributions for these cases is plotted in Fig. 12. Also shown is the PDF obtained by binning the simulation data. Clearly, even this  $2 \times 2$  LIM dynamics obtained by projection on the first two POD modes suffices to predict the observed distribution of the fluctuations.

## V. CONCLUSIONS

It is accepted that the ensemble mean state is a fixed point of the ensemble dynamics to which almost all perturbations relax. It is also believed that sufficiently small perturbations relax following a stable linear dynamics. Recently, IWCV obtained from a perturbed DNS the dominant modes underlying this stable linear dynamics using an ensemble method. However, the interpretation of ensemble dynamics is not straightforward and in this case, as we have shown, the ensemble converges to an unstable repeller rather than to a stable fixed point. This is common in ensemble dynamics, although apparently paradoxical, as the example of the mass-spring with random restoring force governed by the Mathieu equation discussed in the formulation section demonstrates.

It is generally accepted that the ensemble mean state is stable in the sense of linear hydrodynamic stability. However, when account is taken of a set of nonlinear instabilities identified by S3T SSD, it is a repeller in pPf and pCf turbulence. In this paper we have examined the implications of this ensemble mean flow instability for the dynamics of relaxation to the ensemble mean state. In the S3T SSD the mean state is the streamwise average, the fluctuations are the streamwise varying components, and the fluctuation-fluctuation interactions are neglected. A close approximation to the mean flow and the fluctuation covariance in the S3T SSD is obtained from a quasilinear integration of pCf dynamics from which it is verified that the time-mean turbulent state is not a fixed point of the S3T dynamics. Moreover, even if the mean turbulent state is enforced to be an equilibrium, this equilibrium is S3T unstable.

It should be noted that this result applies to the case of post-transitional wall-bounded turbulence and should be contrasted to the case for pretransitional pCf and to the turbulence that occurs in barotropic or baroclinic quasigeostrophic models of planetary turbulence, in which often the time-mean turbulent state is a stable fixed point of both the ensemble and the S3T SSD dynamics. The

SSD fixed point in these cases corresponds, in both the ensemble SSD and the S3T SSD, to the statistical mean turbulent state (up to second-order Gaussian approximation in the case of the S3T SSD). This fixed point solution in the case of the planetary turbulence exhibits the characteristic structure of alternating zonal jets [7,22,77] together with the associated covariances which support the jets by upgradient Reynolds stresses [78]. A familiar physical example of this SSD equilibrium is the zonal jets of Jupiter that have been demonstrated to have a fixed structure over at least decadal periods [79].

The difference between wall-bounded post-transitional turbulence and its pretransitional and planetary counterparts is that, in the latter cases, the S3T SSD has an attracting fixed point which coincides with the ensemble or time-mean state of the turbulence and standard methods of eigenanalysis can be used to obtain the dynamics of perturbations back to the ensemble or time-mean state. In wall turbulence the S3T trajectory lies on a transient chaotic attractor and eigenanalysis of the S3T state cannot be performed to obtain the perturbation dynamics. However, nothing essential is lost because the perturbation dynamics can be obtained by averaging over the transient S3T attractor, which was accomplished using LIM analysis. Our results lend credence to the concept that the fundamental attractor of the turbulent state is identified by the S3T attractor in cumulant variables. When this attractor is visualized in velocity variables it corresponds to a turbulent state with the mean state containing the majority of the energy accompanied by a multivariate elliptical PDF of fluctuations in its immediate vicinity accounting for the remaining energy. Similarly, if we visualize the DNS attractor in velocity variables we find the majority of the energy to be contained in the mean flow with fluctuations in the vicinity accounting for the remaining energy. The S3T attractor identifies the structure and dynamics of this fundamental entity of the turbulence as comprising the first and second cumulants as the fundamental variables, visualized as the mean flow and the surrounding elliptical perturbation distribution, and their interaction as controlling the evolution of the turbulent state in the fundamental SSD variables or equivalently as visualized in velocity variables. Therefore the S3T SSD predicts both the underlying structure and evolution of the turbulent state in phase space.

Similarity between the dynamics of perturbations to the ensemble mean state in S3T SSD simulations, in which the structure and dynamics on the SSD attractor have been explicitly identified, and DNS suggests that the existence of the SSD transient attractor and the concept of averaging over this attractor in order to identify the dynamics of perturbations to the statistical time-mean state extends to DNS. These results suggest that the essentially complete characterization of turbulence in the S3T SSD, and especially the identification of a chaotic attractor in the phase space of its statistical state variables, can be profitably exploited to gain further insight into the dynamics of NSE turbulence.

#### ACKNOWLEDGMENTS

We thank Dr. M.-A. Nikolaidis for making available to us the pPf DNS data.

#### APPENDIX: THE STRUCTURE OF THE RELAXATION DYNAMICS PRODUCED BY LINEAR INVERSE MODEL ON SIX PROPER ORTHOGONAL DECOMPOSITION MODES

When the mean-flow velocity fluctuations are projected on the top six POD modes ordered according to their contribution to the mean fluctuation energy, LIM identifies that the fluctuations are governed by the operator:

$$A_6 = \begin{pmatrix} -0.021 & 0 & 0 & 0.048 & 0 & -0.117 \\ 0 & -0.023 & -0.040 & 0 & -0.004 & 0 \\ 0 & 0.024 & -0.050 & 0 & 0.044 & 0 \\ -0.035 & 0 & 0 & -0.076 & 0 & 0.200 \\ 0 & -0.043 & -0.038 & 0 & -0.091 & 0 \\ 0.024 & 0 & 0 & -0.046 & 0 & -0.239 \end{pmatrix},$$

and are excited by a temporally delta-correlated white-noise forcing with spatial covariance:

$$\Xi_6 = 10^{-5} \begin{pmatrix} 0.177 & 0 & 0 & 0.036 & 0 & 0.013 \\ 0 & 0.15 & 0.04 & 0 & 0.15 & 0 \\ 0 & 0.04 & 0.302 & 0 & 0.05 & 0 \\ 0.036 & 0 & 0 & 0.34 & 0 & -0.094 \\ 0 & 0.15 & 0.05 & 0 & 0.26 & 0 \\ 0.013 & 0 & 0 & -0.094 & 0 & 0.475 \end{pmatrix}.$$

Note that the POD modes, when ordered in variance, have the following symmetry: s, a, a, s, a, s, respectively (“s” denotes symmetry about the  $x$ - $z$  center plane at  $y/h = 1$  and “a” antisymmetry). Because of the statistical symmetry of the fluctuations, interactions among them are restricted to the respective symmetric and antisymmetric subspaces, and consistently the only nonzero entries in the  $A_6$  and  $\Xi_6$  matrices are either in the coordinates of the symmetric modes corresponding to the POD modes 1, 4, 6 or those of the antisymmetric corresponding to the POD modes 2, 3, 5.

That the dynamics is non-normal in the energy inner product can be ascertained by calculating the projections among the eigenmodes indicated by the matrix of the inner product  $u^\dagger u$ :

$$u^\dagger u = \begin{pmatrix} 1 & 0 & 0.3 + 0.3i & 0.3 - 0.3i & 0 & 0 \\ 0 & 1 & 0 & 0 & 0.7 + 0.05i & 0.7 - 0.05i \\ 0.3 - 0.3i & 0 & 1 & 0.3 - 0.3i & 0 & 0 \\ 0.3 + 0.3i & 0 & 0.3 + 0.3i & 1 & 0 & 0 \\ 0 & 0.7 - 0.05i & 0 & 0 & 1 & 0.9 + 0.05i \\ 0 & 0.7 + 0.05i & 0 & 0 & 0.9 - 0.05i & 1 \end{pmatrix}.$$

Here the eigenmodes are ordered increasing in decay rate. The symmetric eigenmodes are 2, 5, 6 and the antisymmetric are 1, 3, 4 and it can be seen, as expected by the statistical symmetry of the dynamics, that non-normal interaction is confined to the mutually orthogonal symmetric and antisymmetric subspaces.

Non-normality of  $A_6$  and noncommutation between  $A_6$  and  $\Xi_6$  results in the POD modes of the Langevin dynamics differing from the eigenmodes of the operator of the dynamics,  $A_6$ , as discussed by North [74] and Monahan *et al.* [75]. However, the statistical symmetry of the dynamics still constrain the POD modes to lie in the mutually orthogonal symmetric and the antisymmetric subspaces of the eigenmodes. The commutator between  $A_6$  and  $\Xi_6$  is

$$[A_6, \Xi_6] = \begin{pmatrix} 0.001 & 0 & 0 & 0.021 & 0 & -0.044 \\ 0 & 0.003 & 0.005 & 0 & 0.006 & 0 \\ 0 & 0.004 & 0.007 & 0 & 0.004 & 0 \\ 0.009 & 0 & 0 & -0.026 & 0 & 0.015 \\ 0 & -0.008 & 0.006 & 0 & -0.01 & 0 \\ -0.015 & 0 & 0 & 0.022 & 0 & 0.025 \end{pmatrix}.$$

The requirement for identity of the POD modes with the modes of the operator in general Langevin dynamics can be immediately seen as follows: the POD modes are the eigenmodes of the fluctuation covariance  $C$ , which is given in Langevin systems by  $\int_0^\infty dt e^{At} \Xi e^{A^\dagger t}$ . Therefore, the eigenmodes of  $C$  coincide with the eigenmodes of  $A$  if  $[A, A^\dagger] = 0$ , i.e.,  $A$  is normal, and  $[A, \Xi] = 0$ , i.e., the forcing does not mix the eigenmodes of  $A$ .

- [1] U. Brosa, Turbulence without strange attractor, *J. Stat. Phys.* **55**, 1303 (1989).
- [2] B. Eckhardt, T. N. Schneider, B. Hof, and J. Westerweel, Turbulence transition in pipe flow, *Annu. Rev. Fluid Mech.* **39**, 447 (2007).
- [3] A. S. Iyer, F. D. Witherden, S. I. Chernyshenko, and P. E. Vincent, Identifying eigenmodes of averaged small-amplitude perturbations to turbulent channel flow, *J. Fluid Mech.* **875**, 758 (2019).
- [4] J. U. Bretheim, C. Meneveau, and D. F. Gayme, Standard logarithmic mean velocity distribution in a band-limited restricted nonlinear model of turbulent flow in a half-channel, *Phys. Fluids* **27**, 011702 (2015).
- [5] B. F. Farrell, P. J. Ioannou, J. Jiménez, N. C. Constantinou, A. Lozano-Durán, and M.-A. Nikolaidis, A statistical state dynamics-based study of the structure and mechanism of large-scale motions in plane Poiseuille flow, *J. Fluid Mech.* **809**, 290 (2016).
- [6] N. C. Constantinou, B. F. Farrell, and P. J. Ioannou, Statistical state dynamics of jet–wave coexistence in barotropic beta-plane turbulence, *J. Atmos. Sci.* **73**, 2229 (2016).
- [7] B. F. Farrell and P. J. Ioannou, Formation of jets by baroclinic turbulence, *J. Atmos. Sci.* **65**, 3353 (2008).
- [8] N. A. Bakas and P. J. Ioannou, Emergence of non-zonal coherent structures, in *Zonal Jets: Phenomenology, Genesis, and Physics*, edited by B. Galperin and P. L. Read (Cambridge University Press, Cambridge, 2019), Chap. 27, pp. 419–436.
- [9] B. F. Farrell and P. J. Ioannou, A stochastic structural stability theory model of the drift wave-zonal flow system, *Phys. Plasmas* **16**, 112903 (2009).
- [10] N. C. Constantinou and J. B. Parker, Magnetic suppression of zonal flows on a beta plane, *Astrophys. J.* **863**, 46 (2018).
- [11] B. F. Farrell and P. J. Ioannou, Dynamics of streamwise rolls and streaks in turbulent wall-bounded shear flow, *J. Fluid Mech.* **708**, 149 (2012).
- [12] B. F. Farrell, P. J. Ioannou, and M.-A. Nikolaidis, Instability of the roll–streak structure induced by background turbulence in pre-transitional Couette flow, *Phys. Rev. Fluids* **2**, 034607 (2017).
- [13] B. F. Farrell and P. J. Ioannou, Structural stability of turbulent jets, *J. Atmos. Sci.* **60**, 2101 (2003).
- [14] K. Srinivasan and W. R. Young, Zonostrophic instability, *J. Atmos. Sci.* **69**, 1633 (2012).
- [15] J. B. Parker and J. A. Krommes, Zonal flow as pattern formation, *Phys. Plasmas* **20**, 100703 (2013).
- [16] N. A. Bakas and P. J. Ioannou, Emergence of large scale structure in barotropic  $\beta$ -plane turbulence, *Phys. Rev. Lett.* **110**, 224501 (2013).
- [17] N. A. Bakas and P. J. Ioannou, On the mechanism underlying the spontaneous emergence of barotropic zonal jets, *J. Atmos. Sci.* **70**, 2251 (2013).
- [18] K. Srinivasan and W. R. Young, Reynold stress and eddy diffusivity of  $\beta$ -plane shear flows, *J. Atmos. Sci.* **71**, 2169 (2014).
- [19] J. B. Parker and J. A. Krommes, Generation of zonal flows through symmetry breaking of statistical homogeneity, *New J. Phys.* **16**, 035006 (2014).
- [20] N. C. Constantinou, B. F. Farrell, and P. J. Ioannou, Emergence and equilibration of jets in beta-plane turbulence: Applications of stochastic structural stability theory, *J. Atmos. Sci.* **71**, 1818 (2014).
- [21] N. A. Bakas, N. C. Constantinou, and P. J. Ioannou, S3T stability of the homogeneous state of barotropic beta-plane turbulence, *J. Atmos. Sci.* **72**, 1689 (2015).
- [22] B. F. Farrell and P. J. Ioannou, Statistical state dynamics based theory for the formation and equilibration of Saturn’s north polar jet, *Phys. Rev. Fluids* **2**, 073801 (2017).
- [23] B. F. Farrell and P. J. Ioannou, Perturbation growth and structure in uncertain flows. Part I, *J. Atmos. Sci.* **59**, 2629 (2002).
- [24] L. Keefe, P. Moin, and J. Kim, The dimension of attractors underlying periodic turbulent Poiseuille flow, *J. Fluid Mech.* **242**, 1 (1992).
- [25] J. Jiménez and P. Moin, The minimal flow unit in near-wall turbulence, *J. Fluid Mech.* **225**, 213 (1991).
- [26] O. Flores and J. Jiménez, Hierarchy of minimal flow units in the logarithmic layer, *Phys. Fluids* **22**, 071704 (2010).



- [27] J. Jiménez and G. Kawahara, Dynamics of wall-bounded turbulence, in *Ten Chapters in Turbulence*, edited by P. A. Davidson, Y. Kaneda, and K. R. Sreenivasan (Cambridge University Press, 2013), Chap. 6, pp. 221.
- [28] M.-A. Nikolaidis, P. J. Ioannou, B. F. Farrell, and A. Lozano-Durán, POD-based study of turbulent plane Poiseuille flow: comparing structure and dynamics between quasi-linear simulations and DNS, *J. Fluid Mech.* **962**, A16 (2023).
- [29] M.-A. Nikolaidis, P. J. Ioannou, and B. F. Farrell, Fluctuation covariance-based study of roll-streak dynamics in Poiseuille flow turbulence, [arXiv:2309.02085](https://arxiv.org/abs/2309.02085).
- [30] Y. Hwang and B. Eckhardt, Attached eddy model revisited using a minimal quasi-linear approximation, *J. Fluid Mech.* **894**, A23 (2020).
- [31] C. G. Hernández and Y. Hwang, Spectral energetics of a quasilinear approximation in uniform shear turbulence, *J. Fluid Mech.* **904**, A11 (2020).
- [32] C. G. Hernández, Q. Yang, and Y. Hwang, Generalised quasilinear approximations of turbulent channel flow. Part I. Streamwise nonlinear energy transfer, *J. Fluid Mech.* **936**, A33 (2022).
- [33] J. U. Bretheim, C. Meneveau, and D. F. Gayme, A restricted nonlinear large eddy simulation model for high Reynolds number flows, *J. Turbul.* **19**, 141 (2018).
- [34] B. F. Farrell and P. J. Ioannou, Statistical State Dynamics: A new perspective on turbulence in shear flow, in *Zonal Jets: Phenomenology, Genesis, and Physics*, edited by B. Galperin and P. L. Read (Cambridge University Press, 2019), Chap. 25, pp. 380.
- [35] V. K. Markeviciute and R. R. Kerswell, Improved assessment of the statistical stability of turbulent flows using extended Orr–Sommerfeld stability analysis, *J. Fluid Mech.* **955**, A1 (2023).
- [36] J. M. Hamilton, J. Kim, and F. Waleffe, Regeneration mechanisms of near-wall turbulence structures, *J. Fluid Mech.* **287**, 317 (1995).
- [37] F. Waleffe, On a self-sustaining process in shear flows, *Phys. Fluids* **9**, 883 (1997).
- [38] C. Penland, Random forcing and forecasting using principal oscillation pattern analysis, *Mon. Weather Rev.* **117**, 2165 (1989).
- [39] C. Penland and M. Ghil, Forecasting northern hemisphere 700-mb geopotential height anomalies using empirical normal modes, *Mon. Weather Rev.* **121**, 2355 (1993).
- [40] C. Penland and P. D. Sardeshmukh, The optimal growth of tropical sea surface temperature anomalies, *J. Clim.* **8**, 1999 (1995).
- [41] T. DelSole, Stochastic models of quasi-geostrophic turbulence, *Surv. Geophys.* **25**, 107 (2004).
- [42] C. Penland and T. Magorian, Prediction of Niño 3 sea surface temperatures using linear inverse modeling, *J. Clim.* **6**, 1067 (1993).
- [43] T. DelSole and A. Y. Hou, Empirical stochastic models for the dominant climate statistics of a general circulation model, *J. Atmos. Sci.* **56**, 3436 (1999).
- [44] C. R. Christopher R. Winkler, M. Newman, and P. D. Sardeshmukh, A linear model of wintertime low-frequency variability. Part I: Formulation and forecast skill, *J. Clim.* **14**, 4474 (2001).
- [45] T. Delsole and B. F. Farrell, The quasi-linear equilibration of a thermally maintained stochastically excited jet in a quasi-geostrophic model, *J. Atmos. Sci.* **53**, 1781 (1996).
- [46] A. Garcöa and C. Penland, Fluctuating hydrodynamics and principal oscillation pattern analysis, *J. Stat. Phys.* **64**, 1121 (1991).
- [47] A. S. Sharma and B. J. McKeon, On coherent structure in wall turbulence, *J. Fluid Mech.* **728**, 196 (2013).
- [48] B. J. McKeon, The engine behind (wall) turbulence: Perspectives on scale interactions, *J. Fluid Mech.* **817**, P1 (2017).
- [49] A. Zare, M. R. Jovanović, and T. T. Georgiou, Colour of turbulence, *J. Fluid Mech.* **812**, 636 (2017).
- [50] A. Towne, A. Lozano-Durán, and X. Yang, Resolvent-based estimation of space–time flow statistics, *J. Fluid Mech.* **883**, A17 (2020).
- [51] H. J. Bae, A. Lozano-Durán, and B. J. McKeon, Nonlinear mechanism of the self-sustaining process in the buffer and logarithmic layer of wall-bounded flows, *J. Fluid Mech.* **914**, A3 (2021).
- [52] P. Morra, P. A. S. Nogueira, A. V. G. Cavalieri, and D. S. Henningson, The colour of forcing statistics in resolvent analyses of turbulent channel flows, *J. Fluid Mech.* **907**, A24 (2021).

- [53] J. J. Holford, M. Lee, and Y. Hwang, Optimal white-noise stochastic forcing for linear models of turbulent channel flow, *J. Fluid Mech.* **961**, A32 (2023).
- [54] J. J. Holford and Y. Hwang, A data-driven quasi-linear approximation for turbulent channel flow, [arXiv:2305.15043](https://arxiv.org/abs/2305.15043).
- [55] S. Abootorabi and A. Zare, Model-based spectral coherence analysis, *J. Fluid Mech.* **958**, A16 (2023).
- [56] J. B. Marston, Atmospheres as nonequilibrium condensed matter, *Annu. Rev. Condens. Matter Phys.* **3**, 285 (2012).
- [57] J. B. Marston and S. M. Tobias, Recent developments in theories of inhomogeneous and anisotropic turbulence, *Annu. Rev. Fluid Mech.* **55**, 351 (2023).
- [58] V. Thomas, B. K. Lieu, M. R. Jovanović, B. F. Farrell, P. J. Ioannou, and D. F. Gayme, Self-sustaining turbulence in a restricted nonlinear model of plane Couette flow, *Phys. Fluids* **26**, 105112 (2014).
- [59] V. Thomas, B. F. Farrell, P. J. Ioannou, and D. F. Gayme, A minimal model of self-sustaining turbulence, *Phys. Fluids* **27**, 105104 (2015).
- [60] B. F. Farrell, D. F. Gayme, and P. J. Ioannou, A statistical state dynamics approach to wall-turbulence, *Philos. Trans. R. Soc., A* **375**, 20160081 (2017).
- [61] F. Alizard, Invariant solutions in a channel flow using a minimal restricted nonlinear model, *Comptes Rendus Mécanique* **345**, 117 (2017).
- [62] F. Alizard and D. Biau, Restricted nonlinear model for high- and low-drag events in plane channel flow, *J. Fluid Mech.* **864**, 221 (2019).
- [63] M. Pausch, Q. Yang, Y. Hwang, and B. Eckhardt, Quasilinear approximation for exact coherent states in parallel shear flows, *Fluid Dyn. Res.* **51**, 011402 (2019).
- [64] W. C. Reynolds and W. G. Tiederman, Stability of turbulent channel flow, with application to Malkus's theory, *J. Fluid Mech.* **27**, 253 (1967).
- [65] D. F. Gayme, B. J. McKeon, A. Papachristodoulou, B. Bamieh, and J. C. Doyle, A streamwise constant model of turbulence in plane Couette flow, *J. Fluid Mech.* **665**, 99 (2010).
- [66] W. V. R. Malkus, Outline of a theory of turbulent shear flow, *J. Fluid Mech.* **1**, 521 (1956).
- [67] B. F. Farrell, P. J. Ioannou, and M.-A. Nikolaidis, Mechanism of roll-streak structure formation and maintenance in turbulent shear flow, [arXiv:2205.07469](https://arxiv.org/abs/2205.07469).
- [68] G. C. Papanicolaou and W. Kohler, Asymptotic theory of mixing stochastic ordinary differential equations, *Commun. Pure Appl. Math.* **27**, 641 (1974).
- [69] T. DelSole, A fundamental limitation of Markov models, *J. Atmos. Sci.* **57**, 2158 (2000).
- [70] C. Penland, The Nyquist issue in linear inverse modeling, *Mon. Weather Rev.* **147**, 1341 (2019).
- [71] T. T. Georgiou, The structure of state covariances and its relation to the power spectrum of the input, *IEEE Trans. Autom. Control* **47**, 1056 (2002).
- [72] A. Zare, Y. Chen, M. R. Jovanović, and T. T. Georgiou, Low-complexity modeling of partially available second-order statistics: Theory and an efficient matrix completion algorithm, *IEEE Trans. Autom. Control* **62**, 1368 (2017).
- [73] G. R. North, T. L. Bell, R. F. Cahalan, and F. J. Moeng, Sampling errors in the estimation of empirical orthogonal functions, *Mon. Weather Rev.* **110**, 699 (1982).
- [74] G. North, Empirical orthogonal functions and normal modes, *J. Atmos. Sci.* **41**, 879 (1984).
- [75] A. H. Monahan, J. C. Fyfe, M. H. P. Ambaum, D. B. Stephenson, and G. R. North, Empirical orthogonal functions: The medium is the message, *J. Clim.* **22**, 6501 (2009).
- [76] S. Russo and P. Luchini, The linear response of turbulent flow to a volume force: Comparison between eddy-viscosity model and DNS, *J. Fluid Mech.* **790**, 104 (2016).
- [77] B. F. Farrell and P. J. Ioannou, Emergence of jets from turbulence in the shallow-water equations on an equatorial beta plane, *J. Atmos. Sci.* **66**, 3197 (2009).
- [78] C. Salyk, A. P. Ingersoll, J. A. Vasavada, and A. D. Del Genio, Interaction between eddies and mean flow in Jupiter's atmosphere: analysis of Cassini imaging data, *Icarus* **185**, 430 (2006).
- [79] A. P. Ingersoll, T. E. Dowling, P. J. Gierasch, G. S. Orton, P. L. Read, A. Sanchez-Lavega, A. P. Showman, A. A. Simon-Miller, and A. R. Vasavada, Dynamics of Jupiter's atmosphere, in *Jupiter: the Planet, Satellites, and Magnetosphere*, edited by F. Bagenal, T. E. Dowling, and W. B. McKinnon (Cambridge University Press, Cambridge, 2004), pp. 105–128.